Available online at www.sciencedirect.com

ScienceDirect

Advances in Space Research 69 (2022) 2283–2304

ADVANCES IN SPACE RESEARCH (a COSPAR publication)

www.elsevier.com/locate/asr

The Ganymede Laser Altimeter (GALA) for the Jupiter Icy Moons Explorer (JUICE): Mission, science, and instrumentation of its receiver modules

Keigo Enya [a,b,*], Masanori Kobayashi [c], Jun Kimura [d], Hiroshi Araki [e,b], Noriyuki Namiki [e,b], Hirotomo Noda [e,b], Shingo Kashima [e], Shoko Oshigami [a], Ko Ishibashi [c], T. Yamawaki [a], Kazuyuki Tohara [a], Yoshifumi Saito [a], Masanobu Ozaki [a,b], Takahide Mizuno [a,b], Shunichi Kamata [f], Koji Matsumoto [e], Sho Sasaki [d], Kiyoshi Kuramoto [f], Yuki Sato [g], Takeshi Yokozawa [g], Tsutomu Numata [g], Satoko Mizumoto [g], Hiroyuki Mizuno [g], Kenta Nagamine [g], Akihiko Sawamura [g], Kazuo Tanimoto [g], Hisato Imai [h], Hiroyuki Nakagawa [h], Okiharu Kirino [h], David Green [i], Masayuki Fujii [j], Satoru Iwamura [k], Naofumi Fujishiro [l], Yoshiaki Matsumoto [m], Kay Lingenauber [n], Reinald Kallenbach [n], Christian Althaus [n], Thomas Behnke [n], Jan Binger [n], Anna Daurskikh [n], Henri Eisenmenger [n], Ulrich Heer [n,o], Christian Hüttig [n], Luisa M. Lara [p], Alexander Lichopoj [n], Horst-Georg Lötzke [n], Fabian Lüdicke [n], Harald Michaelis [n], Juan Pablo Rodriguez Garcia [n,q], Kerstin Rösner [n], Alexander Stark [n], Gregor Steinbrügge [r], Pascal Thabaut [n], Nicolas Thomas [s], Simone del Togno [n], Daniel Wahl [n], Belinda Wendler [n], Kai Wickhusen [n], Konrad Willner [n], Hauke Hussmann [n]

[a] *Institute of Space and Astronautical Science, Japan Aerospace Exploration Agency, 3-1-1 Yoshinodai, Chuo-ku, Sagamihara, Kanagawa 252-5210, Japan*
[b] *The Graduate University for Advanced Studies, SOKENDAI, Hayama, Miura-gun, Kanagawa 240-0193, Japan*
[c] *Planetary Exploration Research Center, Chiba Institute of Technology, 2-17-1 Tsudanuma, Narashino, Chiba 275-0016, Japan*
[d] *Department of Earth and Space Science, Osaka University, 1-1 Machikaneyama-cho, Toyonaka, Osaka 560-0043, Japan*
[e] *National Astronomical Observatory of Japan, 2-21-1 Osawa, Mitaka, Tokyo 181-8588, Japan*
[f] *Department of Earth and Planetary Sciences, Hokkaido University, Kita-10 Nishi-8, Kita-ku, Sapporo, Hokkaido 060-0810, Japan*
[g] *MEISEI Electric Co. Ltd., 2223 Naganuma-cho, Isesaki, Gunma 372-8585, Japan*
[h] *Crystal Optics Inc., 3-4-25 Imakatata, Otsu, Shiga 520-0241, Japan*
[i] *Materion Precision Optics, 2 Lyberty Way, Westford, MA 01886, USA*
[j] *FAM Science Co., Ltd., 2167-1 Tsutsudo, Tsukubamirai, Ibaraki 300-2435, Japan*
[k] *MRJ, 2-16-2, Kugenuma Kaigan, Fujisawa, Kanagawa 251-0037, Japan*
[l] *Astro-Opt, 4-6-7 Sugano, Ichikawa, Chiba 272-0824, Japan*
[m] *PTI Co., Ltd, 5-16-402 Kusunoki-chou, Nishi-ku, Yokohama 220-0003, Japan*
[n] *Institute of Planetary Research, Deutsches Zentrum für Luft- und Raumfahrt, Rutherfordstr. 2, 12489 Berlin, Germany*
[o] *Airbus Defence and Space GmbH, Claude-Dornier-Str., 88090 Immenstaad, Germany*
[p] *Instituto de Astrofísica de Andalucía (CSIC), c/ Glorieta de la Astronomía 3, 18008 Granada, Spain*
[q] *European Space Research and Technology Centre, European Space Agency, Keplerlaan 1, 2200 AG Noordwijk zh, The Netherlands*
[r] *Department of Geophysics, 397 Panama Mall, Mitchell Building, 3rd Floor, Stanford University, Stanford, CA 94305-2215, United States*
[s] *Space Research and Planetology Division, Physikalisches Institut, University of Bern (UBE), Sidlerstrasse 5, 3012 Bern, Switzerland*

Received 6 April 2021; received in revised form 22 October 2021; accepted 28 November 2021
Available online 5 December 2021

* Corresponding author.

https://doi.org/10.1016/j.asr.2021.11.036
0273-1177/

Abstract

The Jupiter Icy Moons Explorer (JUICE) is a science mission led by the European Space Agency, being developed for launch in 2023. The Ganymede Laser Altimeter (GALA) is an instrument onboard JUICE, whose main scientific goals are to understand ice tectonics based on topographic data, the subsurface structure by measuring tidal response, and small-scale roughness and albedo of the surface. In addition, from the perspective of astrobiology, it is imperative to study the subsurface ocean scientifically. The development of GALA has proceeded through an international collaboration between Germany (the lead), Japan, Switzerland, and Spain. Within this framework, the Japanese team (GALA-J) is responsible for developing three receiver modules: the Backend Optics (BEO), the Focal Plane Assembly (FPA), and the Analog Electronics Module (AEM). Like the German team, GALA-J also developed software to simulate the performance of the entire GALA system (performance model). In July 2020, the Proto-Flight Models of BEO, FPA, and AEM were delivered from Japan to Germany. This paper presents an overview of JUICE/GALA and its scientific objectives and describes the instrumentation, mainly focusing on Japan's contribution.

1. Introduction

1.1. Jupiter Icy Moons Explorer (JUICE)

In previous exploration missions to Jupiter, the Galileo spacecraft was the first to remain in the Jovian system to conduct detailed observations (1995 – 2003) (Johnson et al., 1992). One important piece of scientific knowledge implied by this mission is that Jupiter's icy Galilean moons (i.e., Europa, Ganymede, and Callisto) may have a global subsurface ocean (liquid hydrosphere) beneath their icy crust (Kivelson, Khurana, and Volwerk 2002, Schubert et al., 2004). Juno is currently making observations in the Jovian system as well (Bolton et al., 2017). It has been argued that the oceans may have played an important role in the birth and evolution of life on Earth. However, the Earth is currently the only celestial body where the existence of oceans has been confirmed. If the existence of an ocean can be proven in the subsurface of an icy moon, an environment that is completely different from Earth, and the characteristics of that ocean can be clarified, it would also be highly significant from the perspective of astrobiology. It is expected to expand the image of oceans in planetary systems that may provide habitable environments for life other than Earth.

The JUICE is a space mission for Jupiter, its satellites, and magnetosphere. JUICE is led by ESA (Fig. 1) with international collaboration from Japan and the United States (Grasset et al., 2013). The primary goal of JUICE is to explore Jupiter's icy Galilean moons. JUICE will be the first explorer to enter a circular orbit around the moon of a planet other than the Earth's Moon to make detailed observations. In addition, it is the first Jovian system exploration mission led by ESA. JUICE was selected as an L1 mission (the first large-class mission) by ESA's Cosmic Vision in 2012. JUICE will be equipped with 11 scientific instruments.

JUICE will be launched by an Ariane 5 rocket from the Guiana Space Center in 2023 and will swing-by the Earth, Moon, and Venus before reaching the Jovian system in 2031. After this, JUICE will perform multiple flyby observations of Callisto and Europa and enter a polar orbit around Ganymede in 2034. Then, JUICE will observe the entire Ganymede sphere in detail from the orbit at a nominal altitude of 500 km above the surface. The Jovian system's total observation period of JUICE is planned to be

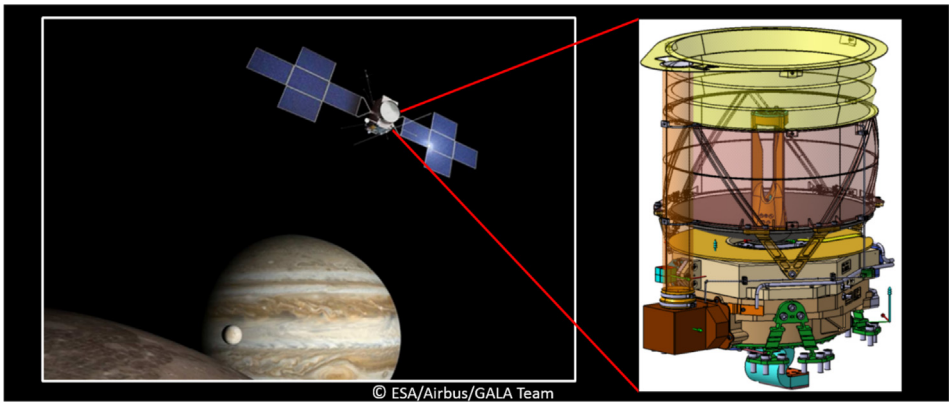

Fig. 1. (Left) Jupiter Icy Moons Explorer (JUICE) and (Right) Ganymede Laser Altimeter (GALA). Right figure from Hussmann et al. (2019).

4 years and 5 months (if resources permit, the mission's life can be extended and observation at a 200 km altitude orbit will be performed).

1.2. Ganymede Laser Altimeter (GALA)

The Ganymede Laser Altimeter (GALA) is one of the scientific instruments mounted on JUICE (Hussmann et al., 2019). The designed outlook of GALA is shown in Fig. 1. The GALA team has set the following key scientific objectives for GALA (Hussmann, 2019, Kimura et al., 2019): (1) Understanding the ice tectonics based on topographic data, (2) Understanding the subsurface structure through tidal response measurements, and (3) Understanding the small-scale roughness and albedo of the surface.

The GALA, developed for the aforementioned scientific objectives, is a single-beam single-detector laser altimeter. Table 1 shows the major specifications of GALA. GALA's main function is to emit highly directional laser pulses (start pulse; energy: 17 mJ, wavelength: 1064 nm, pulse width: 2.9 ns, nominal/maximum frequency: 30 Hz/50 Hz) from orbit onto the icy surface of the moon (nominal spot diameter: ~50 m, nominal spot interval: ~50 m, see Fig. 2), receive the reflected pulses (return pulse) at the receiving telescope (25 cm diameter aperture), and measure the distance (carry out altimetry) from the time lag between the start and return pulses to determine the altitude of the point on the surface where the spot was emitted. At the same time, information on the albedo, slope, and roughness of the observation point can be obtained from the return pulse intensity ratio to the start pulse and the broadening of the pulse width.

Laser altimeters have been developed for planetary exploration missions because of their unique and beneficial features. For example, the Clementine Lidar (Smith et al., 1997), Mars Global Surveyor/ Mars Orbiter Laser Altimeter, MGS/MOLA (Smith et al., 2001), NEAR-Shoemaker/ NEAR Laser Rangefinder, NLR Cheng et al., (2001) Mercury Surface, Space Environment, Geochemistry, and Ranging-Mercury Laser Altimeter, Messenger/MLA (Cavanaugh et al., 2007), KAGUYA/Laser Altimeter, LALT (Araki et al., 2009), Chandrayaan/Lunar Laser-Ranging Instrument, LLRI, (Kamalakar et al., 2009), Hayabusa/Light Detection and Ranging, LIDAR (Mizuno et al., 2010), Chang'E/Laser AltiMeter, LAM (Huang, Ping, & Yan, 2010), Lunar Reconnaissance Orbiter/Lunar Orbiter Laser Altimeter, LRO/LOLA (Smith et al., 2017), Hayabusa2/Light Detection and Ranging, LIDAR (Mizuno et al., 2017), Origins Spectral Interpretation Resource Identification Security-Regolith Explorer (OSIRIS-REx) Laser Altimeter, OLA (Daly et al., 2017), and BepiColombo Laser Altimeter, BELA (Thomas et al., 2021).

Table 1
Main specifications of GALA.

Wavelength	1064.5 nm
Laser energy	17 mJ
Start pulse width	2.9 ns (1σ)
Shot frequency	30 Hz/50 Hz (nominal/maximum)
Beam divergence	100 μrad ($1/e^2$, full cone)
Spot size	50 m ($1/e^2$, diameter, at an altitude of 500 km)
Spot interval	50 m (30 Hz, at an altitude of 500 km)
Telescope aperture	25 cm (diameter)
Field of view	580 μrad (full cone)
Detector	Avalanche Photodiode (APD)
Digital filter	Matched filter
Total mass	24 kg
Size	39 cm × 35 cm × 42 cm
Power consumption	51 W (at 30 Hz)
Altimetry accuracy	1 m (at points with good conditions)

GALA is a laser-ranging instrument (altimeter), like BELA and LIDARs on Hayabusa1 and Hayabusa2, that emits laser pulses to the target and measures the round-trip time and distance for each pulse to the target. These instruments comprise a laser head module, laser collimator (telescope), receiving telescope for the returned pulses, and detector and electronics for the returned pulse detection and data processing, respectively. The range limit of the laser altimeter is determined using the laser pulse energy, beam spreading angle, aperture of the receiving telescope, signal detectability of the detection module (detector and electronics), and albedo/roughness of the target. The ranging accuracy is determined by the timing accuracy of the returned pulses. Topographic resolution is determined by the repetition frequency of pulsed laser emission. The LIDARs onboard Hayabusa1 and Hayabusa2 record the returned pulse intensity as time-integrated energy equivalent data in the detector. At the same time, BELA and GALA enable more accurate ranging and simultaneous measurement of albedo/roughness for each target laser footprint by analyzing the time profile of each returned pulse. Like other instruments mounted on JUICE, GALA will also perform multiple flyby observations of Europa and Callisto and continuously observe Ganymede from a polar orbit at a nominal altitude of 500 km.

As a result, GALA will obtain three-dimensional topographic data and albedo properties across the entire surface of Ganymede and data about time changes in large-scale shapes and orbital motion (surface displacement, phase lag, longitudinal libration; further details in Section 2.2 and Fig. 5). Furthermore, these data are thought to reflect the presence or absence of a subsurface ocean and its characteristics through the tidal effect (see Section 2 for the theoretical expectation values of these quantities).

The GALA is the first laser altimeter to be used on an icy body. It is also the first instrument to take the approach of inferring subsurface structures, such as the presence or absence of subsurface oceans, by measuring large-scale changes in the shape and orbital motion of a celestial body.

1.3. GALA as an international project

The development of GALA is based on an international collaboration between Germany, Japan, Switzerland, and

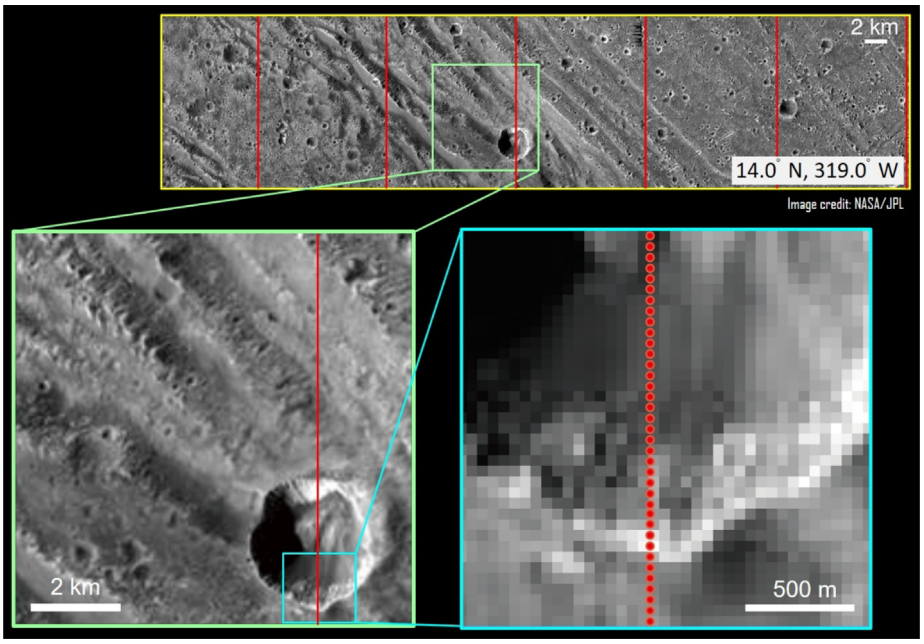

Fig. 2. Approximate distribution of the GALA laser spots in a polar orbit at 500 km altitude shown as red lines and dots on a close-up image of the Ganymede acquired by the Galileo spacecraft. The GALA's trajectory-spacing changes with latitude and is approximately 11 km at 14° N. (The red lines and dots show the approximate trajectory-spacing and the spot interval, respectively, but not the absolute position of them). (For interpretation of the references to colour in this figure legend, the reader is referred to the web version of this article.)

Spain, led by the German Aerospace Center (DLR) (Fig. 3). Germany contributed to the laser systems and associated electronics, the receiving telescope, key electronics and assemblies, and the integration and verification of the entire instrument. The DLR is further responsible for scientific coordination and data analysis, data processing, and archiving by the international GALA team. The Japanese team (GALA-J) is responsible for three hardware modules in the development of GALA: The Backend Optics (BEO), the Focal Plane Assembly (FPA), including the development of the Avalanche Photodiode (APD), and the Analog Electronics Module (AEM). Switzerland and Spain are responsible for the Range Finder Module (RFM) and the Power Converter Module (PCM), respectively. The components for which GALA-J is responsible are located in the core of GALA and include highly sensitive detectors. The development of these components is complex, requiring interdependent optical, electronic, thermal, and mechanical designs within tight constraints.

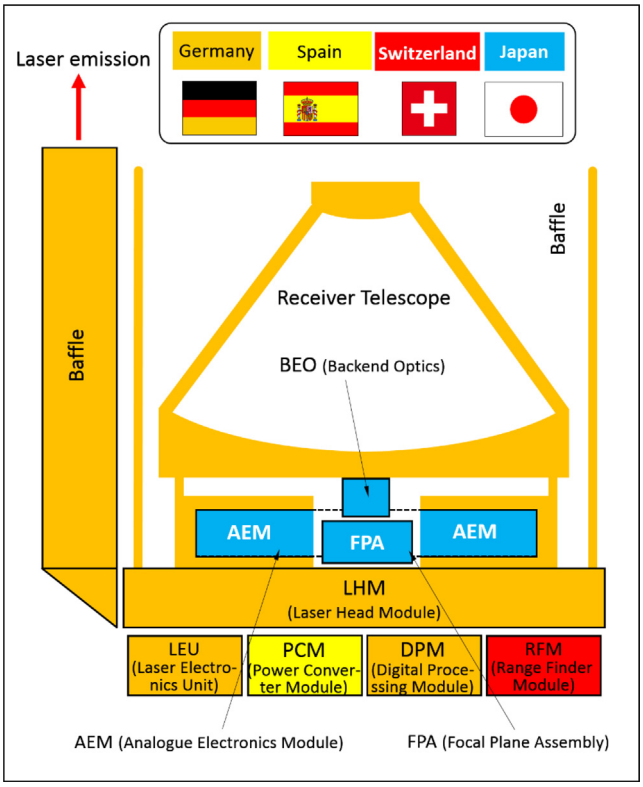

Fig. 3. International work-sharing in GALA equipment development.

The BEO applies spatial and bandpass filters to the return pulses collected by the receiving telescope to increase the signal-to-noise ratio (SNR). The FPA is equipped with an APD sensor module that receives the light emitted from the BEO and outputs an analog electrical signal to the AEM. The FPA is also equipped with two optical fibers (for redundancy). The start pulses sent through these fibers are similarly converted into analog electrical signals and output to the AEM. The primary function of the AEM is to receive the analog signal output from the APD sensor module and convert it into digital signals. The AEM also controls the APD sensor module. Besides the German team, GALA-J has also developed software to simulate

the performance of the entire GALA system (performance model. See also Section 3.2.7).

In July 2020, the Proto-Flight Models (PFMs) of BEO, FPA, and AEM were delivered from Japan to Germany. This paper will provide an overview of JUICE and GALA, their scientific objectives, and instrumentation, emphasizing the parts for which Japan is responsible.

2. Scientific objectives

Observations by GALA, particularly those of Ganymede from a polar orbit, can cover the entire moon with high precision and high sampling density. Furthermore, nine-month observations from the polar orbit allow us to observe with a ground track interval of approximately 8 km on the equator and less than 0.7 km near the poles above 85 latitude. This will provide new insights into icy moons. An overview of the scientific objectives of GALA is given below (see Hussmann et al., 2019; Kimura et al., 2019 for further details).

2.1. Ice tectonics based on topographic data

Icy moons, such as Ganymede, have an icy surface and a structure with various spatial scales that are very different from rocky bodies such as Earth (Figs. 2 and 4). Therefore, detailed measurements of the topography are essential to understand the evolution of icy bodies. However, topographic data to date have been inferior in terms of measurement range, precision, and sampling density. Therefore, observations with GALA will substantially improve this situation (Table 1). The scientific objectives related to ice tectonics based on the GALA topographic data are described below.

2.1.1. Ganymede

Ganymede's surface geology can be divided into three categories: regions with relatively high albedo dominated by channel-shaped structures (Bright Terrain), regions saturated with impact craters with relatively low albedo (Dark

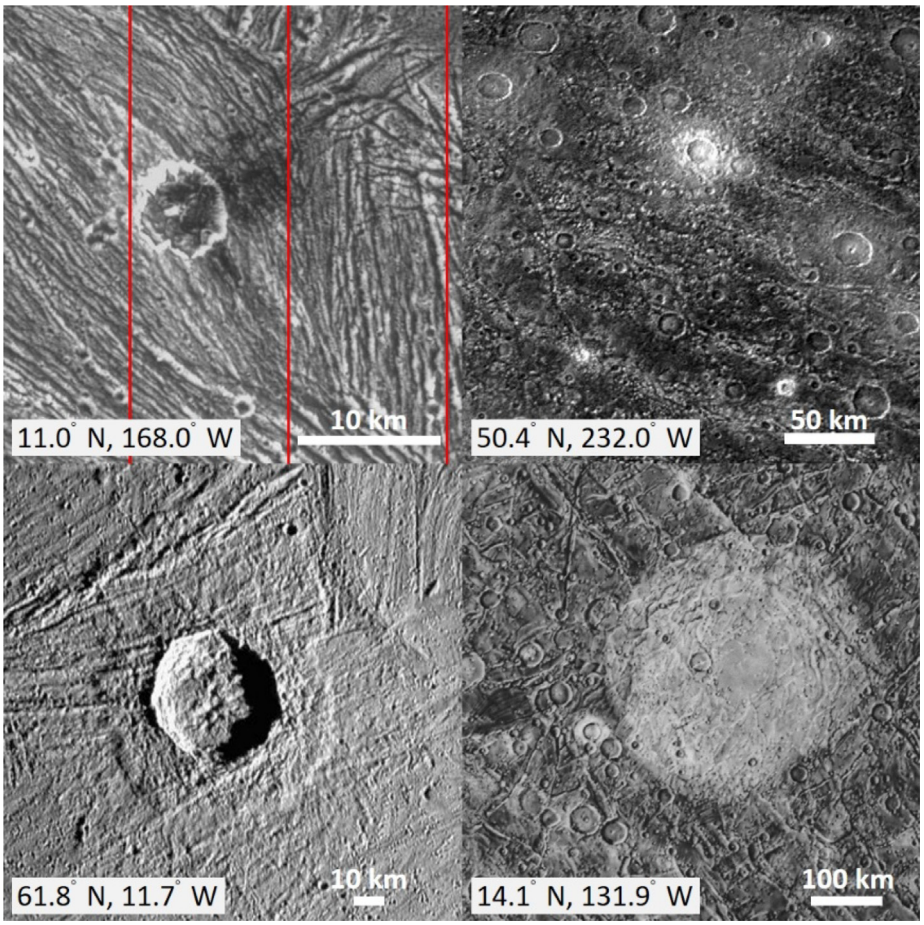

Fig. 4. Typical geology of Ganymede. Top left: Groove (Uruk Sulcus) in Bright Terrain. Top right: Fossae (Lakhmu Fossae) in Dark Terrain. Bottom left: Impact crater (Achelous crater) with a diameter of 40 km. Bottom right: Old impact feature whose topography has disappeared as the relaxation progressed (Memphis Facula) with a diameter of 360 km. Red lines in the top left: Approximate distribution of GALA laser spots on a polar orbit at an altitude of 500 km. The GALA's trajectory-spacing varies with latitude (e.g., ~11 km (top left), 7.6 km (top right), 5.5 km (bottom left) and 11.4 km (bottom right)). Because there are too many trajectories to display, they are omitted except for the top left corner. (For interpretation of the references to colour in this figure legend, the reader is referred to the web version of this article.)

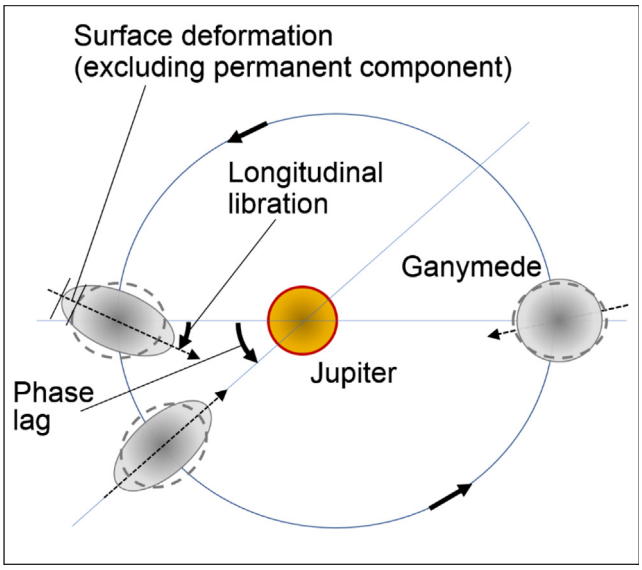

Fig. 5. Conceptual diagram of surface deformation, phase lag, and longitudinal libration. The relative size and distance between Jupiter, Ganymede, and its orbit are not to scale, but the physical quantities are emphasized.

Terrain), and structures formed by the impact of celestial bodies (impact structures).

(1) Bright Terrain

These regions with relatively higher albedo (a bolometric albedo of around 0.5–0.6 (de Kleer et al., 2021)) are characterized by a channel-shaped topography, termed Grooves (groups of Grooves are termed Sulcus). Bright Terrain makes up around 2/3 of Ganymede's surface (Fig. 4). These regions commonly consist of closely spaced, parallel to sub-parallel grooves. Each groove has a topographic wavelength of the order of 1 km and a height of several tens to hundred meters. Some major grooves are as long as several thousand kilometers.

Since the grooves have a fracturing morphology of pre-existing old terrains, they are interpreted as groups of normal faults produced by surface tensile stress. On Earth, stress generation and subsequent tectonic activity are characterized by the formation, movement, and subduction of tectonic plates. In contrast, no such structures and activities have been found on Ganymede. On the icy surface, global expansion due to changes in internal temperature, phase changes in water, and upwelling plumes due to solid-state convection of ice have been proposed as the sources of stress (Showman and Malhotra, 1997; Bland and Showman, 2007).

GALA will perform global measurements of Ganymede with high spatial resolution and high accuracy. Based on these data, the thickness of the elastic lithosphere and the total global expansion can be evaluated through the quantitative morphological analysis of the grooves. We can also estimate the volumetric expansion required for Bright Terrain formation, i.e., the internal temperature change or solidification of the subsurface ocean can also be inferred, providing important information for constraining the internal thermal history. Furthermore, by identifying small impact craters in combination with high-resolution images acquired by the visible camera (JANUS, Jovis, Amorum ac Natorum Undique Scrutator), the surface geological age can be more accurately determined. By combining morphological, stratigraphic, and age data for each terrain, our understanding of the Ganymede ice tectonics will be greatly enhanced.

(2) Dark Terrain

Regions with relatively low albedo (mean albedo at 1 μm is about 0.25) are saturated by impact craters and are presumed to be very old (at least 4 Gyr) (Zahnle et al., 2003). Thus, Dark Terrain makes up about one-third of Ganymede's surface. In addition, the trough-like features called Furrows (regions dominated by multiple Furrows are called Fossae), which appear to overlap with existing impact craters, have a similar morphology to Grooves. Although the formation process for Fossae is unclear, they are related to multiple ring structures formed by colossal impact events because the distribution of Furrows appears to be concentric circles (Hirata et al., 2020). Furthermore, the internal volume changes that formed grooves in the Bright Terrain could also create structures in Dark Terrain. Thus, they might have been mixed with Furrows that were formed by impact events. To clarify the origin of Furrows, the formation process of Dark Terrain must be elucidated by combining the Furrow topographic data obtained by GALA, geological age estimation by analyzing the size and frequency distribution of impact craters using high-resolution images taken by visible cameras, and the compositional analysis of Dark Terrains using near-infrared spectroscopy.

(3) Impact Structures

The morphology of impact craters on Ganymede varies as the size increases and the shape changes from simple bowl-like, flat-bottomed, central-peak, central-pit, or dome types to complex/multi-ring structures. Similar trends are also observed on Callisto and Europa. However, the number of craters differs between these moons, being less on Europa and more on Callisto. Moreover, the ratio of depth to diameter in large craters is small, indicating that such craters have a shallow floor (Schenk, 2002).

Such trends for the size and depth of craters depend on the amount of viscous relaxation and associated long-term morphological changes. In general, larger craters relax more rapidly than small craters because of isostatic adjustments. The degree of viscous relaxation is determined by the thickness of the lithosphere, which is controlled by the heat flow from the interior. Accordingly, the degree of relaxation for craters (especially larger ones) is an essential clue for constraining the interior thermal evolution.

Furthermore, as viscous relaxation proceeds, changes in the stress field may cause the formation of faults. The formation of faults within craters (concentric multi-ring or radial linear features) is also controlled by the thickness of the lithosphere.

The combination of high-resolution images and topographic information obtained by GALA is essential to investigate crater relaxation. In addition, the accurate determination of the ratio of depth to diameter for small craters, which are almost unrelaxed, is important for estimating the relaxation degree of large craters.

2.1.2. Europa and Callisto

The JUICE spacecraft plans to fly by Europa twice. During each flyby, GALA will perform altimetry when the spacecraft altitude is 1300 km or less. Although Europa's surface has a wide variety of geological structures similar to Ganymede, its age is estimated to be considerably younger than that of Ganymede (typically about 40 Myr) (Zahnle et al., 2003). Its surface geology can be divided into three categories: first, linear structures called Lineaments; second, locally fractured terrain, called Mottled Terrain; and third, impact structures.

For Callisto, the JUICE spacecraft will perform 10 flybys or more. During each flyby, GALA will carry out altimetry when the spacecraft altitude is 1000 km or less. Impact structures globally dominate Callisto's surface, and the geological age is estimated to be more than 4 Gyr (Zahnle et al., 2003).

The observations of Europa and Callisto by JUICE will be limited during the flybys, and therefore the surface coverage will significantly be reduced compared to the global observation of Ganymede. However, the GALA measurements and associated investigations using other instruments onboard the JUICE spacecraft will substantially improve our current understanding of Europa and Callisto.

2.2. Subsurface probed by tidal response measurements

As in the Earth-Moon system (Araki et al., 2009), tides caused by gravitational interactions between Jupiter and its moons induce periodic variations in the shape and motion of the planet and its moons (Fig. 5). The amount of tidal response depends on the composition and internal structure of the moon. Theoretical calculations predict that the tidal response differs significantly depending on the presence or absence of subsurface oceans (Kamata et al., 2016). Continuous altimetry for monitoring the overall shape of the moon and the periodic time-variability of the various anomalies of the moon's orbit around Jupiter can measure surface displacements (radial variation) and rotational changes (libration, which is the horizontal shift of the surface) due to tides.

2.2.1. Surface displacements

Although previous observations have suggested the existence of subsurface oceans in the icy moons of Jupiter, no specific evidence or detailed understanding of the ocean has been established (Schubert et al., 2004; Saur et al., 2015). Therefore, GALA will attempt to confirm the presence or absence of such oceans and determine their characteristics using altimetry for the first time.

The amplitude of surface deformation due to tides is theoretically predicted to be different in the case of a liquid ocean and in the case where the entire H_2O layer is solid and mechanically attached to a deep rock layer (Kamata et al., 2016). In the presence of a subsurface ocean, the displacement Love number (h_2) is in the range 1.0 to 1.7, and the phase lag (the angle between the perijove and the orbital position where the displacement is maximum, see also Fig. 5) is 10° or less. On the other hand, when there is no ocean, h_2 ranges from 0.1 to 1.6, and the phase lag can be as much as 60° (Kamata et al., 2016). The current GALA performance model estimates the relative accuracy of h_2 to be about 2% (Steingrugge et al., 2015).

Uncertainties in the estimation of tidal Love number are mainly due to the unclear thickness, viscosity, and rigidity of the ice shell. For example, if the viscosity of the high-pressure ice layer is low, h_2 is enlarged even in the absence of a subsurface ocean. This means that the presence or absence of a subsurface ocean cannot be determined only by the displacement Love number. Therefore, measuring phase lags and tidal amplitudes is critical for inferring the presence or absence of a subsurface ocean in Ganymede.

2.2.2. Rotational change

Ganymede is in a synchronous rotational state, and its orbital period is the same as the spin period on average. Europa and Callisto also rotate in the same way. Although the moon orbits with the same face to Jupiter, the tidal torque from Jupiter changes its spin rate (forced libration, See also Fig. 5). In general, the magnitude of forced libration depends on the internal structure. For example, Ganymede's forced libration is estimated to be about 6.5 to 9 m at its equator, depending on the presence or absence of a subsurface ocean (Steinbrügge et al., 2015; 2019). The measurement accuracy of libration is estimated to be 6.6–17.4 m using JUICE–GALA (Steinbrügge et al., 2019) or 2 μrad (~5.2 m) using JUICE-3GM (Gravity & Geophysics of Jupiter and Galilean Moons) (Cappuccio et al., 2020) at the equator which can constrain the thickness of an elastic ice shell with an accuracy of 24–63 km (Steinbrügge et al., 2019). Therefore, it may be possible to determine the presence of a subsurface ocean only from librational measurements. GALA measurements alone are insufficient to determine the magnitude of libration, but combined with measurements of the tidal displacement Love number h_2, they can provide valuable constraints on the outer ice shell.

Moreover, information on the rotational state will be a prerequisite for determining Ganymede's body-fixed frame and consequently accurate mapping of its surface. It will provide fundamental information for geodetic measurements with the radio science experiments (3GM) and the

altimetry that is accurate for the forced libration of 2 μrad (~5.2 m) (Cappuccio et al., 2020) at the equator. Therefore, it will be possible to determine the presence or absence of a subsurface ocean only from librational measurements.

2.3. Small-Scale roughness and albedo

Information on the surface condition can be obtained from the broadening and intensity of return pulses relative to the start pulses of GALA. Detail of this topic will be presented in a forthcoming paper in preparation by the GALA team. Therefore, this section gives an overview.

2.3.1. Small-Scale surface roughness

Data provided by GALA enable us to quantitatively investigate small-scale roughness and its dependency on geological units and external processes such as sublimation due to solar insolation and plasma sputtering. For Ganymede, the latitudinal and longitudinal distributions of small-scale roughness will also be measured throughout the global observation. This study aims to understand the fundamental topographical changes caused by external factors and their timescales (space weathering rate).

2.3.2. Surface albedo

The average albedo of icy Galilean moons is highest on Europa, followed by Ganymede, and lowest on Callisto. Albedo varies by geological unit, with older units having lower albedo. Furthermore, there are significant differences in albedo between the leading and trailing hemispheres because of sputtering by high-energy particles within the Jovian magnetosphere. In Ganymede, the albedo at 1.0 μm is about 0.52 and 0.44 for leading and trailing hemispheres, respectively (Calvin et al., 1995). In addition, Ganymede has an intrinsic magnetic field created by dynamo motion in the metallic core and bright features in the polar regions referred to as "polar caps." Sputtered ice by plasma is considered to migrate to locally colder areas in the polar region (Khurana et al., 2007). The global albedo measurement with GALA at a laser wavelength of 1064 nm is independent in an insolation condition and provides zero-phase reflectance data. This will help us understand the origin of albedo contrast owing to the radiation and ultraviolet light. The forthcoming manuscript will address the reflectance precision of GALA and its dependency on small-scale surface roughness.

2.4. Synergy with other instruments

Image data obtained from the JANUS (Jovis, Amorum ac Natorum Undique Scrutator) visible light camera puts the GALA measurements into a geological context. It can be combined with altimeter data to detect rotational changes more accurately. Since tidal deformation also produces temporal changes in the gravity field, the measurements of tidal potential by radio science experiments (3GM, Gravity & Geophysics of Jupiter and Galilean Moons) and the altimetry of GALA provide detailed constraints on the Love numbers. Investigating near-surface mass distribution anomalies through gravitational measurements by 3GM and subsurface structure by radar instruments, RIME (Radar for Icy Moons Exploration), which will penetrate the ice layer, will contribute to understanding the ice shell structure and its tectonic activity, combining the laser altimetry of surface topography. Visible and infrared imaging spectrometers, MAJIS (Moons and Jupiter Imaging Spectrometer), ultraviolet spectrograph, UVS, and the sub-millimeter wave instrument obtain information related to the surface and atmospheric composition at various wavelengths. In addition, the magnetometer J-MAG (JUICE magnetometer) monitors the electromagnetic induction of the moon due to variations in the magnetic field of Jupiter. J-MAG will obtain information about the size and composition (electrical conductivity) of the subsurface ocean, with supporting observations from the non-thermal neutral particle detector, particle environment package (PEP), and radio and plasma wave investigation (RPWI).

It will also be important to coordinate with ground-based telescopes and other space probes. Such a comprehensive approach will advance the perspective of planetary science and astrobiology. We believe that the information provided by GALA and JUICE will be an important milestone in the study of extrasolar planetary systems, icy bodies, astrobiology, and in the elucidation of the overall picture of planetary systems in the universe.

3. Instruments

3.1. GALA functions and components

GALA's functions and specifications are outlined in Section 1. The GALA hardware consists of multiple modules as shown in Fig. 3. Definition of abbreviations for name of the modules are described in its caption. The functions of each module are described below in the order of the signal flow (See Hussmann et al. (2019) for further details).

- LHM•LEU: Generates start pulses.
- Emitter Telescope: Collimate the laser beam to irradiate the surface of a celestial body, such as Ganymede, with generated laser pulses.
- Receiver Telescope: Receives and concentrates the return pulses reflected from the surface of the celestial body being observed and feeds it to the BEO.
- BEO: Performs spatial filtering using a pinhole and wavelength filtering using a bandpass filter so that return signals can be received with a high SNR.
- FPA: Houses the APD sensor module. The return pulse emitted from the BEO is converted from an optical signal into an analog electrical signal using the APD detector. Two optical fibers (for redundancy) feed a small fraction of the start pulse into the FPA.

- AEM: Controls the APD sensor module and converts the analog electrical signal output from the FPA into digitized pulse waveform.
- RFM: Receives the digital signal output from the AEM and determines the time lag between the start and return pulses and the waveform and intensity of the return pulse.
- DPM: Controls the instruments and serves as the interface with the spacecraft.
- PCM: Supplies power to GALA at various voltages.

3.2. Developments in Japan

GALA-J is responsible for the three modules BEO, FPA (including the APD sensor module), and AEM in the international hardware development process (Fig. 3). Furthermore, a performance model (software) has been developed by the GALA-J team to verify the requirements and assess the resulting quality of the GALA measurements.

3.2.1. Requirements for development in GALA-J

In the entire GALA project, requirements for the development of instruments were defined to realize the performance of GALA (Table 1). Using a performance model (Section 3.2.7), GALA-J determined detailed requirements in developing the BEO, FAP, and AEM to satisfy the overall instrument requirements. Major requirements for developing GALA-J are summarized in Table 2, together with achieved performance.

3.2.2. Model Philosophy: Developed models (Hardware) and their objectives

In developing space instruments, multiple hardware models are generally fabricated at different stages for various purposes. Table 3 summarizes the BEO, FPA, and AEM models developed by GALA-J, their aims (model philosophy), and the final delivery destination. The simulators shown in Table 3 are hardware models developed to be exchanged among international partners to ensure interface consistency and usage in verification experiments.

3.2.3. BEO

The BEO is a module used to filter and focus the optical signals collected by the receiving telescope. The function of the BEO is to perform spatial and wavelength filtering to detect return pulses with a sufficiently high SNR. The optical design and the mechanical design of the BEO are shown in Figs. 6 and 7, respectively (see also Enya et al., 2018).

The entrance aperture of the BEO is a pinhole with a diameter of 700 μm. The mechanical interface between the German-made side (the receiving telescope side) and the BEO was set so that the pinhole aperture was located at the focal point of the receiving telescope. This pinhole performs the role of spatial filtering. The required f-number of the light after passing through the pinhole is 4.5. The first lens collimates return pulses entering the BEO through the pinhole to perform high-precision wavelength filtering, passing through a bandpass filter. Then, the image is reconstructed by the second lens (Figs. 6 and 7).

The number of lenses (made of quartz) was minimized to two and both sides of each lens were treated with an anti-reflection coating to realize the required efficiency of the optical system. The alignment tolerance between the BEO and FPA is secured by designing an optical system as a reduction lens (magnification 0.52). A retaining structure that does not use adhesive and a matching special lens shape were designed and fabricated to implement this optical system within the design constraints (Figs. 6 and 7). The implemented anti-reflective coating has a reflectivity of 0.05 % or less (the requirement was 0.5 % or less) per surface, which is sufficiently low (Table 2).

The encircled energy was experimentally measured from images of the BEO pinhole aperture, as shown in Fig. 8. The size of the pinhole aperture (i.e., hardware aperture) was fixed throughout this experiment. In the analysis of each obtained image, the encircled energy (the energy contained in a circle on the image) was evaluated as a function of the diameter on the image. As a result, it was confirmed that the plots of experimental data before and after the vibration tests were in good agreement with the design values.

As shown in Fig. 9 and Table 2, the bandpass filter achieved a good transmissivity of 96 % on average (the required value was 90 %) through the entire required transmission wavelength range (1064.53 ± 1.5 nm). The transmission curve of the bandpass filter was designed to cover this required transmission wavelength range with a margin. As a result, the manufactured bandpass filter achieved high transmissivity in the 4 nm bandwidth as designed. The measured optical density (OD) of the bandpass filter was more than six (the requirement was five) in the blocked wavelength range with the lower and upper wavelength limits of 300 and 1200 nm, respectively (Fig. 9 and Table 2).

The BEO housing was designed to act as a radiation shield. Its shape and thickness were determined to satisfy the radiation shielding requirements of the internal optical devices. The BEO housing also serves as a high-precision mechanical interface with the German-made telescope. In order to realize these properties, the BEO housing was designed and fabricated as a machined part from a single piece of material by high-precision machining using stainless steel (SUS316) as the base metal. Passivation treatment was applied to the surface of the BEO housing. Furthermore, part of the external surface of the BEO housing was coated with gold to consider the thermal radiation properties (Fig. 7). In the BEO, a path was created to allow the air in the space inside the housing to escape during launch. This path was designed to go through multiple bends before exiting to prevent the ingress of stray light.

Table 2
Major requirements for the development of GALA-J for the BEO, FPA, and AEM.

Module	Parameter	Requirements	Achievements
BEO	Lens surface reflectivity	$< 0.5\%$/surface[1]	$< 0.05\%$/surface
	Focusing quality	Encircled energy $> 99\%$	$\sim 100\%$
	Transmissivity of the bandpass filter at its pass band	$> 90\%$ (average) at $\lambda = \lambda c \pm 1.5$ nm[2]	$> 95\%$
	Blocking of the bandpass filter	OD > 5 at $300 < \lambda < (\lambda c - 4.5)$ nm, $(\lambda c + 4.5) < \lambda < 1200$ nm	OD > 6
		OD > 2 at $(\lambda c - 4.5) < \lambda < (\lambda c - 3.2)$ nm, $(\lambda c + 3.2) < \lambda < (\lambda c + 4.5)$ nm	OD > 2
FPA	Responsivity of APD sensor	> 700 kV/W	750 kV/W @ 1060 nm
	Module bandwidth	> 90 MHz	> 100 MHz
	Noise floor level at the TIA output	< 40 fW/$\sqrt{\text{Hz}}$ in NEP for an entire bandwidth of 100 MHz	27 fW/$\sqrt{\text{Hz}}$ in NEP for an eintire bandwidth of 100 MHz
AEM	Noise floor level at the input to the ADC[3]	< 40 fW/$\sqrt{\text{Hz}}$ in NEP	39 fW/$\sqrt{\text{Hz}}$ in NEP
	ADC sampling rate	$\geqq 200$ Msamples/s	200 Msamples/s
	ADC dynamic range	12 bits	12bits
	Cut-off frequency for analog signal line for -3 dB gain	$\leqq 100$ kHz and $\geqq 100$ MHz	Lower limit: 50 kHz Upper limit: 100 MHz
Assembly	Temperature (T)[4]	BEO + FPA -35 °C < T<+85 °C (Non-operational) -25 °C < T<+50 °C (Operational) AEM -35 °C < T<+65 °C (Non-operational) -5°C < T<+45 °C (Operational)	Qualified by environmental tests
	Mass	$\leqq 351$ g for BEO + FPA $\leqq 474$ g for AEM	328.9 g 407.9 g
	Power	$\leqq 9.7$ W TEC in operation[5]	
		FPA + AEM	8.79 W
		AEM only	8.46 W
		FPA only	0.33 W
		TEC not in operation	
		FPA + AEM	6.69 W
		AEM only	6.40 W
		FPA only	0.18 W

1) It means totally $< 2\%$ for two lens optics with four surfaces.
2) λ is the wavelength, and $\lambda c = 1064.53$ nm. For achieved performances of the bandpass filter, see also Fig. 9.3) Analog-to-Digital Converter.4) Acceptance level (See also Table 5).
5) Power when the APD temperature is controlled to 25 °C, and the APD case is 50 °C.

In the BEO design cycle, a tolerance (allowance error) analysis was carried out considering factors such as the manufacturing precision, the alignment precision, thermal expansion of all parts, and the temperature dependence of the refractive index. The results of the tolerance analysis were fed back into the design. As a result, alignment and retention of the internal parts of the BEO, such as lenses, bandpass filters, spacers, and springs, are ensured only by assembling them using screws (no need for adhesives or internal fine optical adjustments). The BEO housing was slightly oversized for the diameter of all lenses, bandpass filters, spacers, and springs. This diameter margin and the packing method using the springs in the BEO release stress caused by thermal expansion (or contraction) of the BEO housing and internal parts. In addition, temperature variation causes shifting in the focus position. However, as shown in Fig. 6, this shift is negligible, and the BEO optics is designed to absorb the effect of the shift by the alignment margin defined on the detector surface (see Fig. 6).

On the other hand, for the alignment of BEO and FPA, we thought mechanical adjustment was necessary based on the tolerance analysis results. In particular, it was needed to achieve fine alignments in the XY-direction by measuring the optical performance for in-plane shifting in the XY-direction (the optical axis was taken as the Z-direction). Hence, a degree of freedom was created for mechanical adjustment between the BEO and FPA (Fig. 7). The XY-adjustment was executed so that the center of the APD detector inside the FPA is on the optical axis of the BEO with a sufficiently high precision of ± 25 μm. Furthermore, since the image of the pinhole of the BEO needed to be formed on the APD detector of

Table 3
Models (hardware) developed by GALA-J and their purposes[1)].

Module	Model	Purpose	Usage location / organization
BEO and FPA	STM1	Structure and Thermal Model-1. Prototyping of mechanical interface and surface treatment for structural and thermal testing.	Japan
	STM2	Structural and Thermal Model-2.	DLR → ESA
	S05	STM simulator (for testing by international partners)	DLR → HDT*
	EM1-1	Engineering Model-1–1. Electrical model of detector peripherals	DLR → ESA
	BEO standalone model**	Prototyping of fabrication, verification, and environmental testing of the optical system	Japan
	EM1-2	Engineering Model-1–2. Verification of thermal design of detector peripherals	Japan
	EM1-3	Engineering Model-1–3. A model with the same design as PFM. Improve surface treatments. Establish design and procedures for manufacturing and assembling PFM. Establish testing methods and testing equipment, advance verification of function, and performance feasibility for PFM	Japan (loaned to DLR, HDT later)
	PFM	Proto-Flight Model	DLR → ESA
	FS	Flight Spare	DLR → ESA
AEM	BBM	Feasibility demonstration using commercially available parts	Japan
	STM	Structural and Thermal Models.	DLR → ESA
	AEM SIM	Simulator (for testing by international partners)	DLR → University of Bern
	EM1-1	Engineering Model-1–1. For system tests	DLR → ESA
	EM1-2	Engineering Model-1–2. For confirming interface with RFM	Japan
	EM1-3	Engineering Model-1–3. For confirming interface with RFM and verifying design	Japan
	PFM	Proto-Flight Model	DLR → ESA
	FS	Flight Spare	DLR → ESA

*Hensoldt Optronics (Germany): Main contractor company for GALA in Germany.
** This model is for the BEO only and does not include the FPA.

the FPA, the alignment in the Z-direction (distance between the BEO and the FPA) needed to be adjusted separately from the receiving telescope. However, its required accuracy was not high. Therefore, the use of spacers was enough to fix the distance between the BEO and the FPA. The tolerance analysis confirmed that the adjustment of tip and tilt between the BEO and the FPA was not necessary. In addition, measures against stray light were taken between the BEO and FPA, in which the stray light path was designed to go through multiple bends before reaching the outside.

Qualification tests were conducted on the lenses and bandpass filter in terms of radiation, temperature, and humidity. In addition, radiation analysis was carried out (see Section 3.2.6), and the analysis results were fed back into the design. Based on these results, the design cycle was iterated so that the BEO housing and internal structure also fulfilled a radiation shielding function, and the shielding requirements were completely satisfied.

All functions and performance values were experimentally verified by developing EM1-3 with the same design as the PFM (Table 3). Then, based on EM1-3 and previous models, the PFM was developed and tested with full consideration of product and quality assurance. Fig. 10 shows an image of the external appearance of the fabricated BEO + FPA Flight Model (PFM). The mass of the manufactured BEO and FPA was 328.9 g and included the optical fibers, thermal straps, and electric harnesses (measured at the configuration shown in Fig. 7 and the top panel of Fig. 10).

3.2.4. FPA

The FPA is a module that contains the APD sensor module, including the APD sensor and its peripheral devices (Fig. 7). The primary role of the FPA is to receive the optical signal (return pulse and part of the start pulse) and convert them into an electrical signal.

The return pulses are fed into the FPA via the receiving telescope and BEO and are incident on the APD sensor. The FPA also has two optical fibers for introducing a small fraction of the photons of the start pulse. The two fibers were used to ensure redundancy. The fiber used was Rad-Hard 62.5/125 micron Multimode Fiber (MIL-PRF-49291/6) made by DRAKA. Its core diameter, cladding diameter, and numerical aperture are 62.5 μm, 125 μm, and 0.275, respectively.

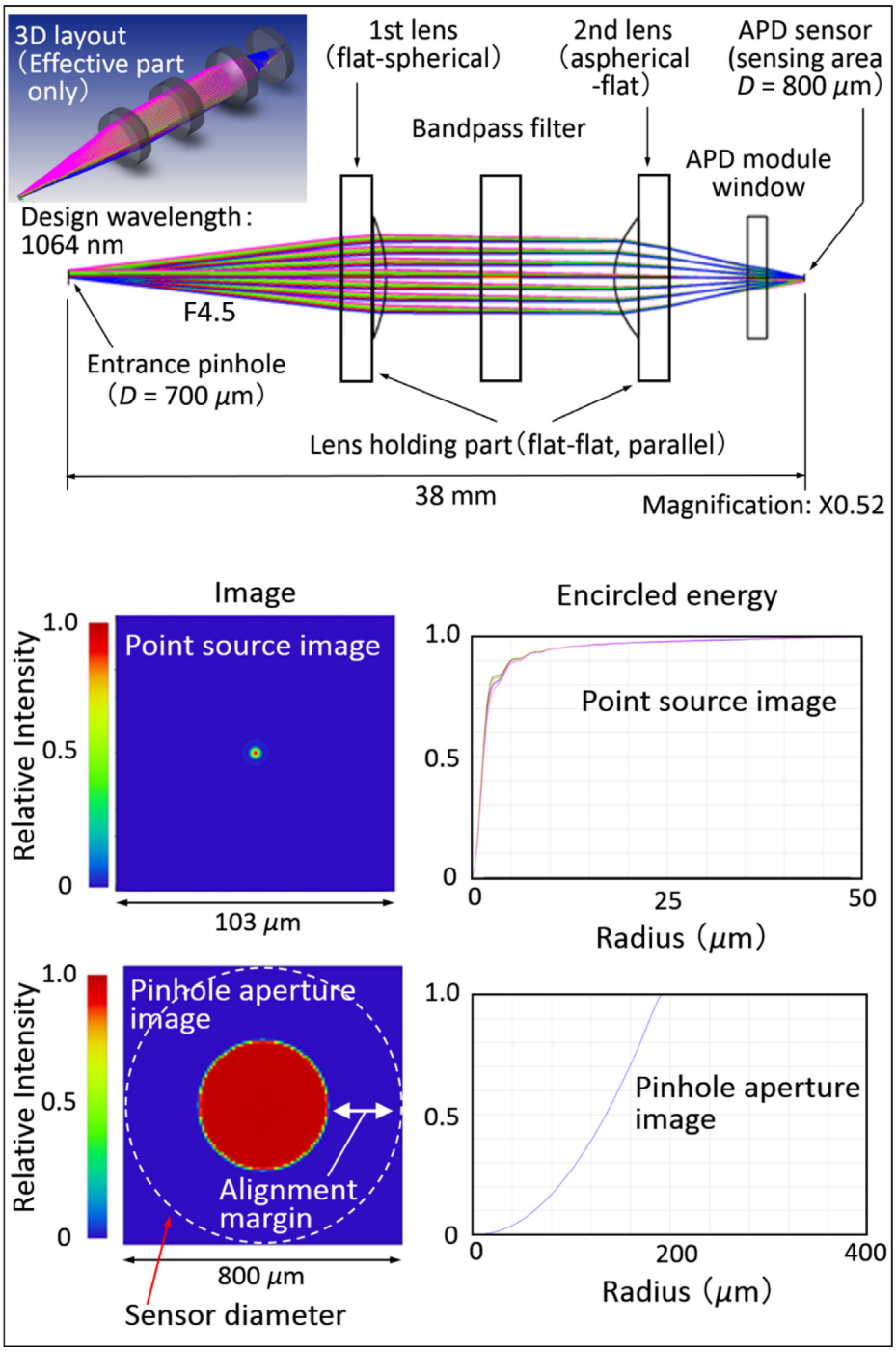

Fig. 6. BEO optical design. The upper part shows the design of the lens optics, and the lower part shows the imaging properties.

The photons fed into the FPA through the optical fiber pass through a small ball lens to reduce the beam diffusion angle. They are reflected from two small metal mirrors and reach the APD sensor (Fig. 11). Installing a regular mirror inside the FPA was difficult due to space limitations. Accordingly, the mirror was designed to be part of an internally fitted structural component. Hence, a reflective path was created by polishing and coating a small part of the structural component with gold. This system enabled us to detect the time lag and intensity ratio for the return pulse relative to the start pulse and the pulse width broadening by the same detector. The output signal from the APD sensor is amplified by a trans-impedance amplifier (TIA) with a bandwidth of 100 MHz in the APD sensor module and output to the AEM.

The APD sensor module in GALA was developed based on a commercially available product by Excelitas Technologies Corp., LLAM-1060-R8BH. In order to satisfy the performance required by the GALA team and meet environmental tolerance as needed for the JUICE mission,

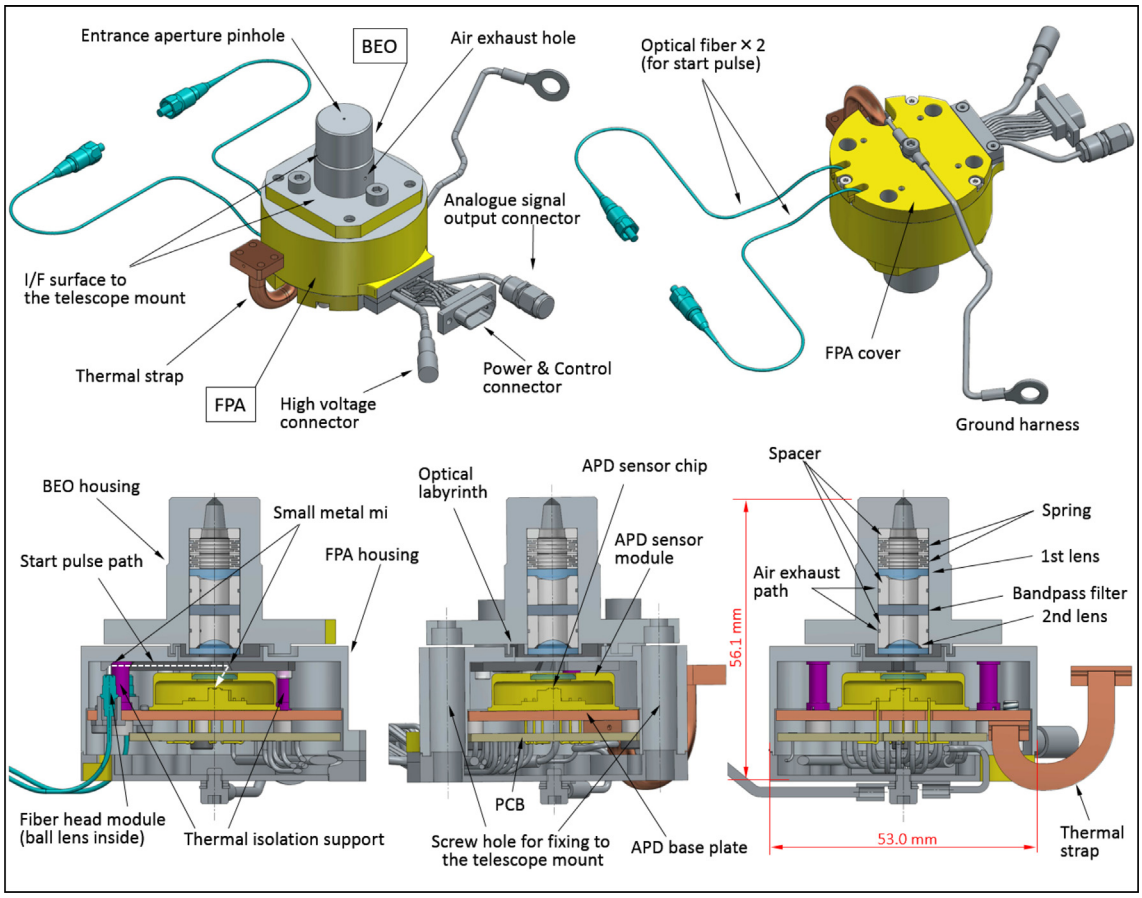

Fig. 7. External (top) and cross-section (bottom) views of the BEO and FPA.

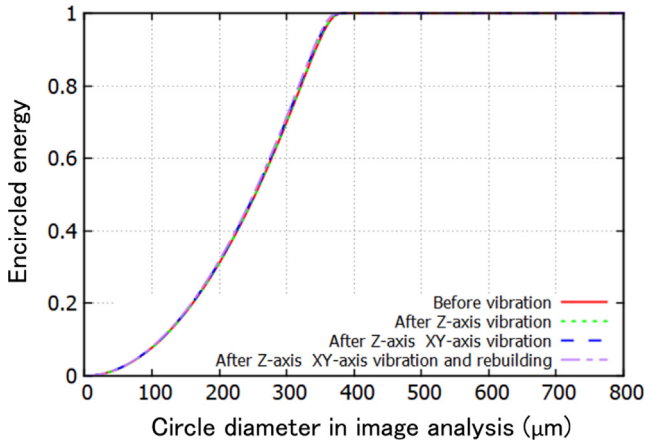

Fig. 8. Experimentally measured encircled energy obtained from the images of the pinhole aperture of the BEO.

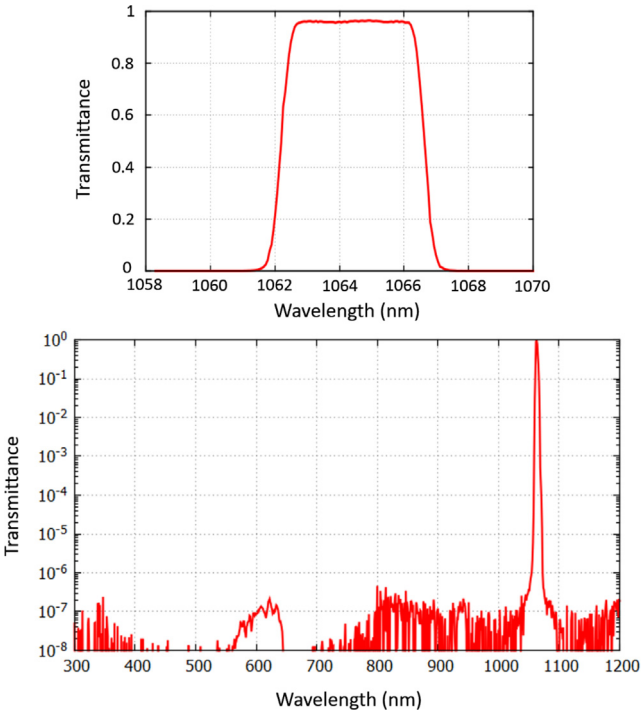

Fig. 9. Experimentally measured transmittance of the bandpass filter.

Excelitas Technologies Corp. redesigned the APD module and accomplished the campaign of qualification tests of it. Although the APD sensor used is a commercial product, it was carefully selected from a controlled manufacturing lot dedicated to GALA development to meet the required specifications shown in Table 2. In addition, the TIA built into the APD module as a pre-amplifier was designed and

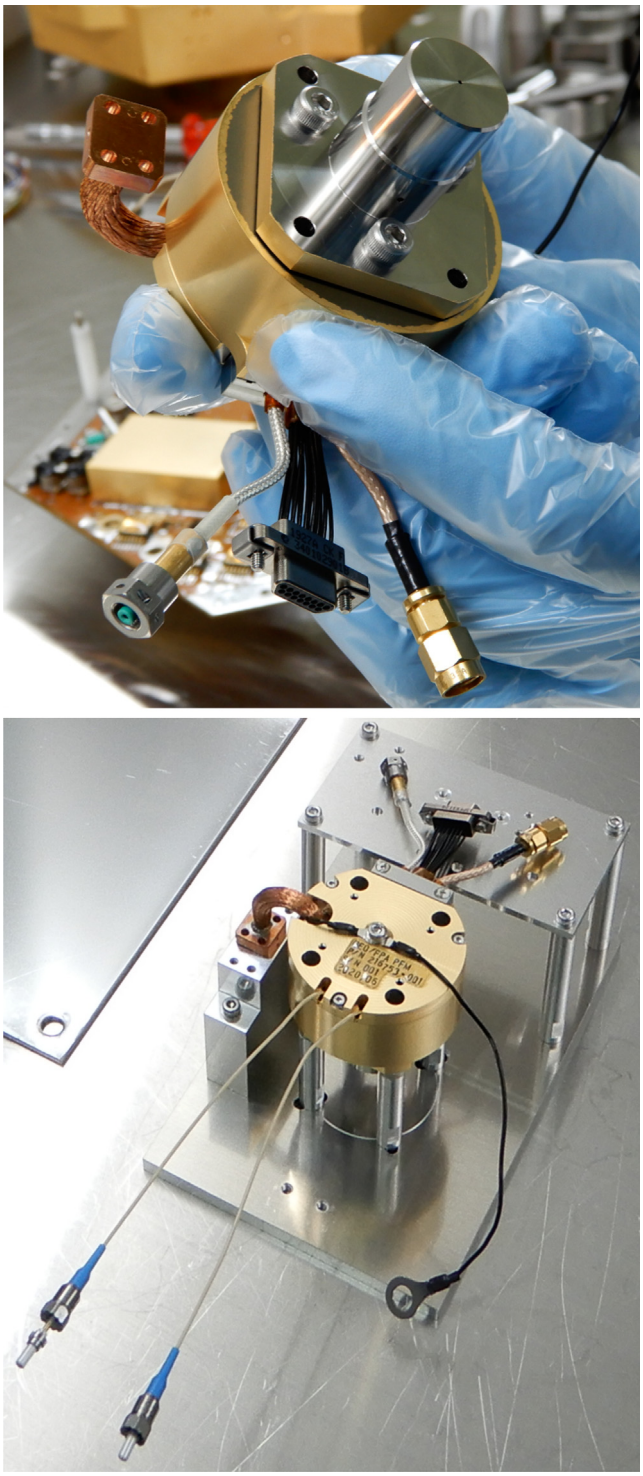

Fig. 10. The external appearance of BEO + FPA FM.

manufactured to meet the bandwidth, gain, and noise level requirements.

This APD sensor (C30954E, Si APD) made by Excelitas Technologies Corp. is known to have high detection efficiency at the fundamental wavelength of YAG lasers (1064.5 nm), as described by Laforce (2009). Moreover, it has a successful track record in many previous space missions. For example, This sensor was also used in the LALT onboard the Kaguya mission (Araki et al., 2009) and the LIDAR onboard the Hayabusa 2 mission (Mizuno et al., 2016).

Although the APD sensor can amplify small optical signals by the avalanche effect inside the sensor, it has been known that the amplification ratio and noise level are highly temperature-dependent. Therefore, the APD sensor in GALA is packaged in a compact module housing (diameter around 1 in.) with a pre-amplifier, a Peltier device for APD temperature control, and a temperature sensor mounted on a single circuit board as a hybrid IC (Fig. 7). This contributes to preventing external noise contamination, highly accurate temperature control, and overall compactness of the FPA and GALA.

In developing the APD sensor module, a serious problem was performance degradation due to high-intensity electron beams in the Jovian magnetosphere. Therefore, an electron beam irradiation test was executed at ONERA, French Aerospace Lab, to investigate the radiation tolerance of the APD sensor. Proton irradiation test was also carried out at the radiation laboratory in the National Institute for Quantum and Radiological Science and Technology in Japan and the cobalt irradiation facility at Tokyo Institute of Technology, Japan.

We conducted GEANT4 (Geometry and Tracking code, version 4, in Agostinelli et al., 2003; Allison et al., 2006; Allison et al., 2016) numerical simulations assuming the JUICE environment (JUICE team, 2017), the detailed

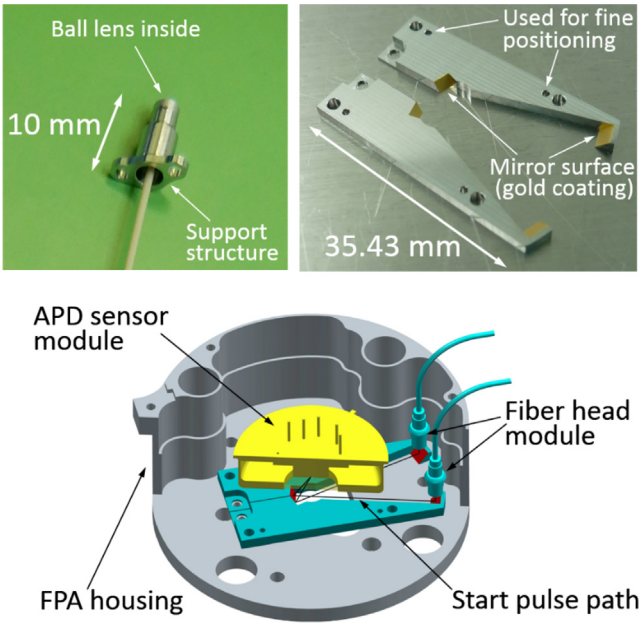

Fig. 11. Top left: Fiber head module with a fiber and support structure. Top right: SUS316 PFM components, of which small flat surfaces are used as mirrors in the FPA. The mirror surfaces were polished and coated with gold. Bottom: Optical paths for introducing a small fraction of the photons of the start pulse to the APD sensor viewing from the backside of the FPA. Only selected parts of the FPA are shown. The APD sensor module is schematic.

structure of the spacecraft, and GALA's modules in the vicinity of APD. Based on these simulations, the rate of energetic electrons passing through the sensors is estimated to be 1.94×10^{-1} electrons/s in the Ganymede orbit. Therefore, when energetic electrons pass through the APD sensor, the signal output from the APD sensor may be falsely detected as a received signal. In order to evaluate the aliasing induced by energetic electron beams, we conducted electron beam irradiation tests using the LINAC accelerator at Kyoto University Research Reactor Institute (now the Institute for Integrated Radiation and Nuclear Science, Kyoto University, Japan). As a result, it was found that the APD signal caused by the passage of the electron beam is a very short pulse of a few ns width, and the risk of it being falsely detected as the received signal from Ganymede is very low. Such a short pulse could be falsely recognized as a start pulse if judged by the pulse shape alone. However, the start pulse is always synchronized with the timing signal of the laser excitation. Therefore, the asynchronous pulse signal can be easily identified as a false signal. Furthermore, we believe that the possibility of noise excited by multiple electron beam simultaneously is very low.

Qualification tests of the optical fiber in terms of radiation, temperature, and humidity, were conducted in Japan. A radiation analysis was carried out (see Section 3.2.6), and the analysis results were compared with the test results described above, which was fed back into the design. Based on these results, the design cycle was iterated so that the FPA housing and internal structure had a radiation shielding function, and the shielding requirements were completely satisfied. Similar to the BEO, the FPA housing is made of stainless steel (SUS316). Passivation treatment was applied to its surface. Furthermore, part of the outer surface of the FPA housing was coated with gold in consideration of the thermal radiation properties (Fig. 7).

The thermal design of FPA, which had to be consistent with the structural, mechanical, and optical design in a limited space, was a challenging issue. It was necessary to make the FPA operational and storable in a significantly changing temperature environment (see Table 2). Internal parts of the FPA must be thermally insulated from the FPA housing, which is thermally connected to the receiving telescope. In addition, it is essential to achieve a capacity for exhaust heat to keep the APD operational at the operating temperature (25 °C) while maintaining the flexibility of the thermal strap. Fig. 12 shows the thermal strap and path for exhausting heat from the APD. The twisted wire of the thermal strap and blocks at both ends were made of copper. To achieve high thermal conductivity, the twisted wire and blocks were joined by soldering. The X-ray inspection images of the thermal strap show that there are no voids in the solder joints, and the area where the solder has soaked into the twisted wire is small. The APD module and APD base plate have adhered using STYCAST 2850 (0.1 mm thickness). The thermal strap and the APD plate are fixed by a combination of adhering (STYCAST 2850, 0.1 mm thickness) and screwing. For electric grounding, the APD sensor module and APD base plate are electrically connected by conductive adhesive (ABLESTIK 56CJ) at two points. The thermal strap and APD base plate are electrically connected via screws.

These functions and performance parameters were experimentally verified by developing EM1-3 with the same design as the PFM (Table 3). Then, the PFM was developed and tested based on the EM1-3 and previous models, but considering the full product and quality assurance (Fig. 10).

3.2.5. AEM

The AEM has two major roles. The first is to drive the APD sensor module to operate under suitable conditions for light pulse measurements. The AEM has a high-voltage circuit for applying a reverse bias voltage to the APD sensor, which is controllable in the range of 300 V to 400 V in 1-V steps to obtain the best responsivity of the APD sensor. The AEM also has a thermal control circuit for driving a Peltier device to control the temperature of the APD sensor to stabilize the signal gain since it is strongly temperature-dependent.

The second role of the AEM is to convert the analog signal that the APD sensor outputs via the TIA (continuously varying in a bandwidth of 100 MHz) into digital data using an ADC circuit and send it to the RFM in real time. To ensure that the output signal of the APD module does not degrade, we implemented an analog signal line with a gain control amplifier and differential conversion circuit from one, which leads the APD output signal to the ADC circuit. As a result, the noise level of the input signal of the ADC was 39 fw/$\sqrt{}$Hz at NEP, and the noise at the APD output signal was 27 fw/$\sqrt{}$Hz at NEP, meeting the requirements shown in Table 2. The requirements were also met for the gain flatness of $\pm$ 0.5 dB in the entire bandwidth from 100 kHz to 100 MHz and the gain of – 3 dB at 100 MHz relative to 400 kHz. The ADC circuit uses two 100-Msps ADCs and samples the waveform of the APD sensor signal at 200 Msps with 12-bit resolution using a time-interleaved method in which the sampling timing of each ADC is shifted by 180°.

Fig. 13 shows the functional block diagram of the AEM: the outputs of the two ADCs (ADC0 and ADC1) are transmitted to the RFM via J2 and J3 connectors synchronously as 24-bit data with a 100 MHz clock frequency. Fig. 14 shows the appearance of the AEM, which is a circuit board attached to flat cables. The AEM is built into a structure that serves as an optical bench for the receiving telescope in the entire GALA.

In order to implement the above functions, the AEM receives a $\pm$ 7 V DC power supply from the PCM via the RFM. The AEM also receives commands from the DPM via the RFM and sends control and housekeeping data back to the RFM to monitor the status of the above functions.

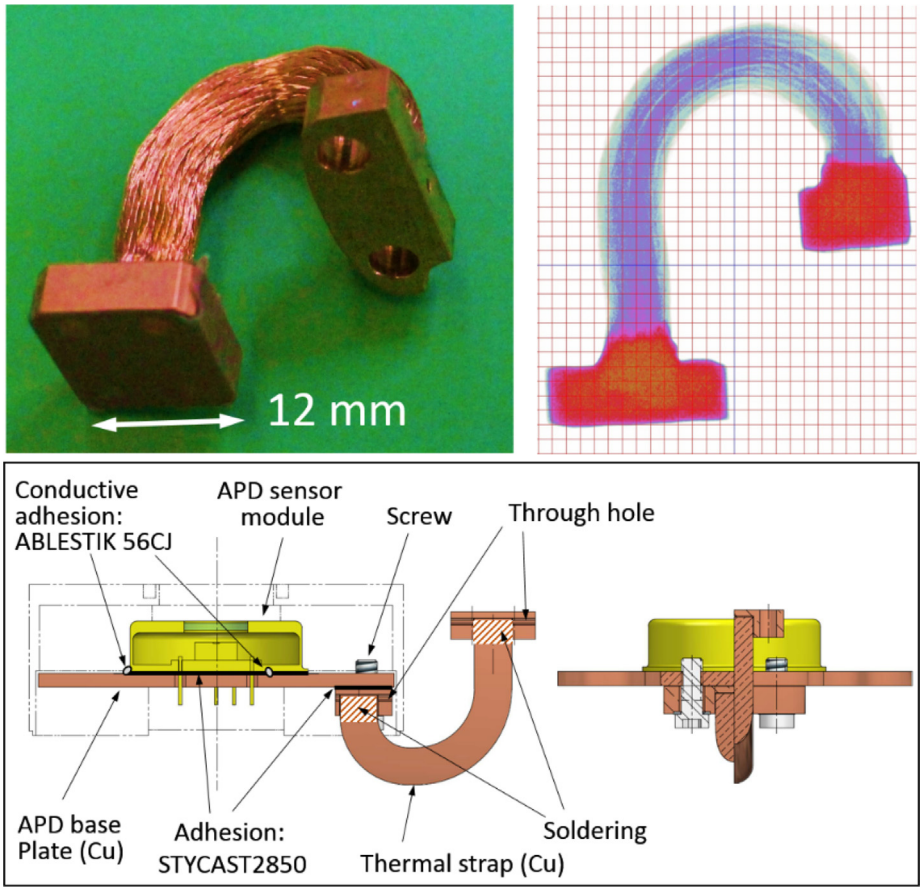

Fig. 12. Top left: The thermal strap of the PFM. Top right: An X-ray image showing the PFM thermal strap. No void was found in the solder joint part, and the area soaked with solder is small. Bottom: The thermal path from the APD sensor module to the thermal strap. Only selected parts of the FPA are shown. The APD sensor module is schematic.

3.2.6. Radiation analysis

The JUICE spacecraft is expected to be exposed to a severe radiation environment in the Jovian magnetosphere, where electrons and protons are magnetically trapped, and the solar and galactic protons are magnetically shielded. This is a unique radiation environment, where the flux of electrons is larger than the flux of protons. Therefore, the onboard instruments must have appropriate radiation shielding based on the environmental radiation conditions specified for the JUICE mission (JUICE team, 2017). On the other hand, the modules that GALA-J is in charge of developing (BEO/FPA/AEM) have limitations in terms of acceptable size and mass. Hence, it was necessary to design the modules so that their housings and built-in components could shield radiation. As a result, radiation analysis by numerical simulations played an important role in designing the structure of the modules and the arrangement of the components while evaluating the radiation shielding effects.

The main components of the environmental radiation in the Jovian magnetosphere are energetic electrons and protons trapped in a strong magnetic field. The radiation environment in JUICE is different from that in interplanetary space, mainly characterized by solar protons and galactic cosmic rays. The JUICE radiation environment is predominantly composed of electrons. It has a fluence higher than the total fluence of solar protons and traps Jovian protons by a factor of 100, particularly at energy levels between 10 keV and 200 MeV. Consequently, these high-energy electrons account for most of the total ionizing dose (TID) (refer to JUICE team, 2017).

Unlike gamma rays, high-energy electrons induce displacement damage (DD). Consequently, there are concerns about the performance degradation of electronic parts such as bipolar transistors and optoelectronic components such as high-sensitivity photodetectors. A 1 MeV electron induces a DD about two orders of magnitude lower than a 1 MeV proton of the same fluence. However, electrons can penetrate deep into shielding. For example, a 3 mm aluminum plate can shield 25 MeV protons while only shielding electrons up to 1 MeV (Ziegler, SRIM Software, 2013; Ester Program, 2017). Thus, they can easily reach radiation-sensitive electronic components deep inside the spacecraft structure.

Assuming that GALA is onboard the JUICE spacecraft, radiation analyses of BEO, FPA, and AEM were performed. The analysis software used was FASTRAD 3.7.0 (Reverse Monte Carlo). Fig. 15 shows the geometry model used in the analysis. In this model, the outer structures of

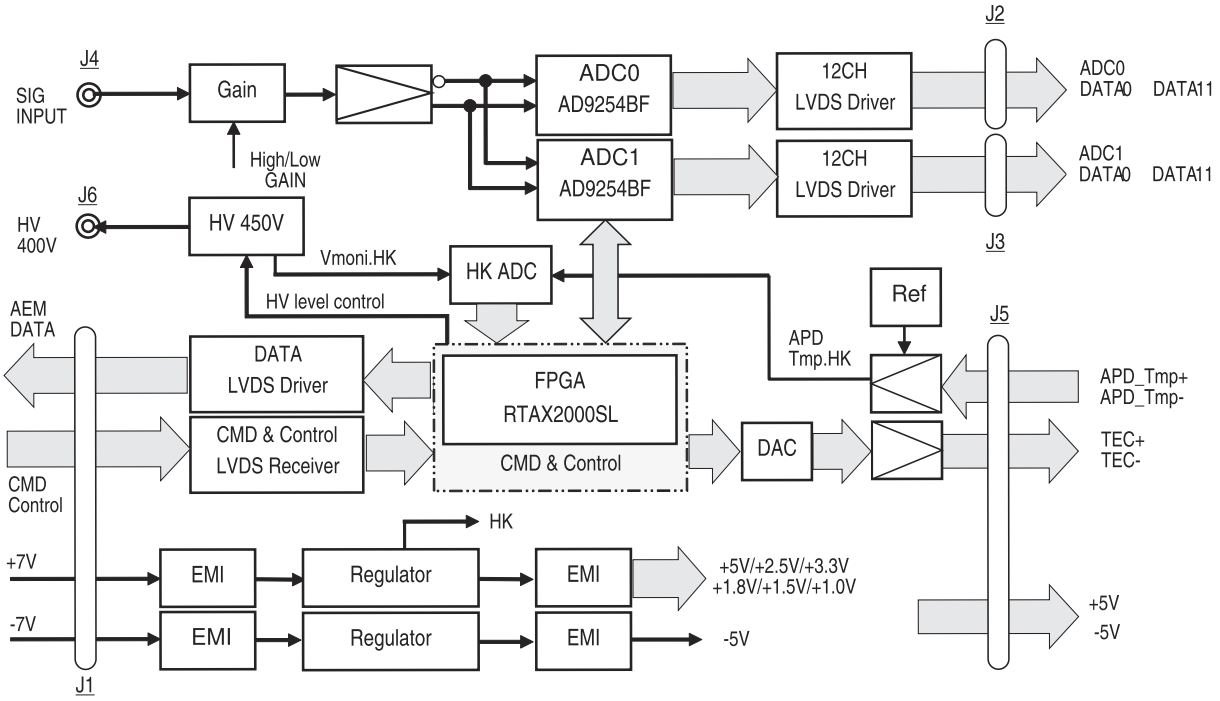

Fig. 13. Functional block diagram of the AEM. The following are expansions of the abbreviations used in the diagrams; ADC: Analog-to-Digital Converter, CMD: Command, DAC: Digital-to-Analog Converter, EMI: Electromagnetic Interference filter, FPGA: Field Programmable Gate Array, HK: Housekeeping data, HV: High-Voltage supply, LVDS: Low Voltage Differential Signaling, Vmoni.HK: Voltage monitor Housekeeping data.

the FPA and BEO (housing, bolts, etc.) were made of SUS316. The housing of the APD sensor module of the FPA was made of Kovar. Finally, the APD sensor (Excelitas Corp., C30954E, diameter: 0.8 mm, thickness: 0.05 mm) of the APD sensor module was fabricated to full scale by simulation. Although the actual APD sensor module contains electronic components, a Peltier device and some leads wires, they were omitted from the model in this analysis. The only primary particles simulated as radiation environments were electrons and protons, while electrons, protons, and photons (gamma rays) were considered secondary radiation species.

The calculated TID of the optical components in the BEO was 12 krad for the first lens, 9 krad for the second lens, and 9 krad for the bandpass filter. Assuming that the lifetime of the APD sensor module is 13.5 years and the safety factor is 2, the calculated TID and TNID (radiation absorption including DD effect) were 15 krad and 1.2×10^7 MeV/g, respectively. However, the actual radiation tests using the electron beam from the ONERA 2 MeV electron accelerator showed that the TID and TNID were 30 krad and 1.0×10^8 MeV/g, respectively. The large difference between the estimated and tested values is because the shielding assumed in the preliminary dose estimation before radiation testing was aluminum, whereas the final shielding was stainless steel.

The radiation resistance of the components used in the BEO and FPA has been confirmed by the manufacturer's warranty or radiation testing by GALA-J to exceed the above doses by an appropriate margin. The analysis of the AEM showed a large change in the dose depending on the position of the AEM (Fig. 15). The dose of the AEM increased toward the edge, reaching a maximum of 155 krad. Therefore, the fixation to the case was accomplished at the edge of the circuit board, and radiation-sensitive electronic components were placed in the center where the dose was low. As a result, all components of the AEM had radiation tolerance exceeding the environmental dose with an appropriate margin. Finally, the designs of the BEO, FPA, and AEM satisfying radiation tolerance were obtained from the above study.

3.2.7. Performance model (Simulation software for entire GALA)

The performance model refers to the software that simulates the performance of the entire GALA. It plays an essential role in checking and configuring requirements in the development, designing hardware, and evaluating test results in the GALA project. Accordingly, in addition to the German team, GALA-J has developed a performance model (Araki et al., 2019) for flexible use and double-checking in GALA-J. This was used in the instrumentation of BEO, FPA, and AEM. An example of the use of this performance model is also given below.

The values stipulated in the GALA performance requirements are range accuracy and probability of false detection in the case of Ganymede polar orbit observations and Europa flyby observations (Table 4). GALA uses waveform data to detect the peak time of the return pulse. Therefore, the four range accuracy and requirements for the probability of false detection in Table 4 can be traced back to scientific requirements as follows. Case A: Success-

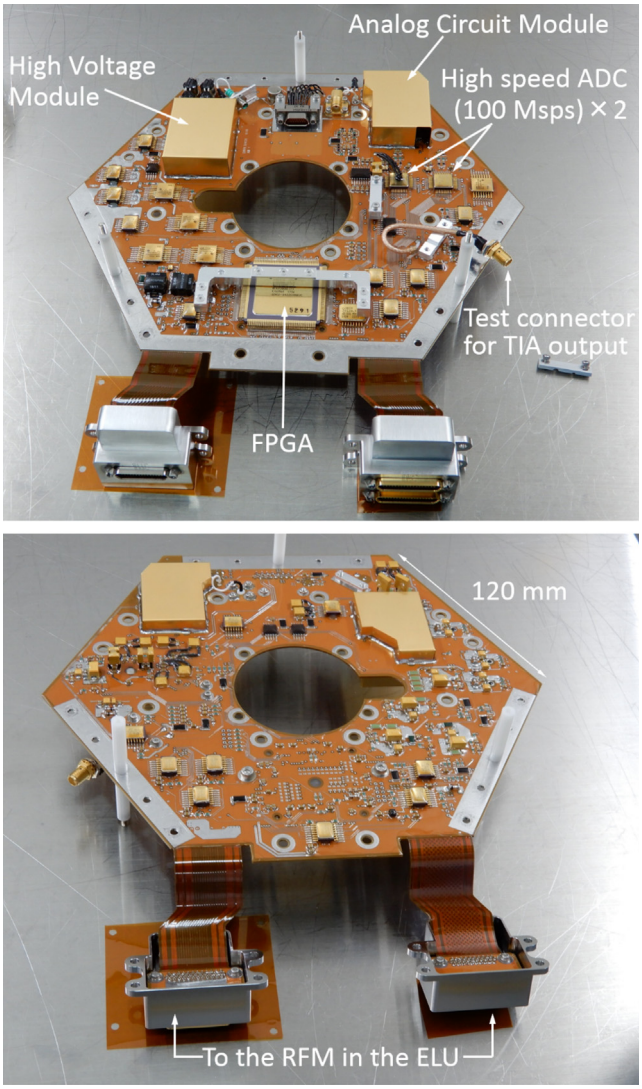

Fig. 14. The external appearance of the AEM.

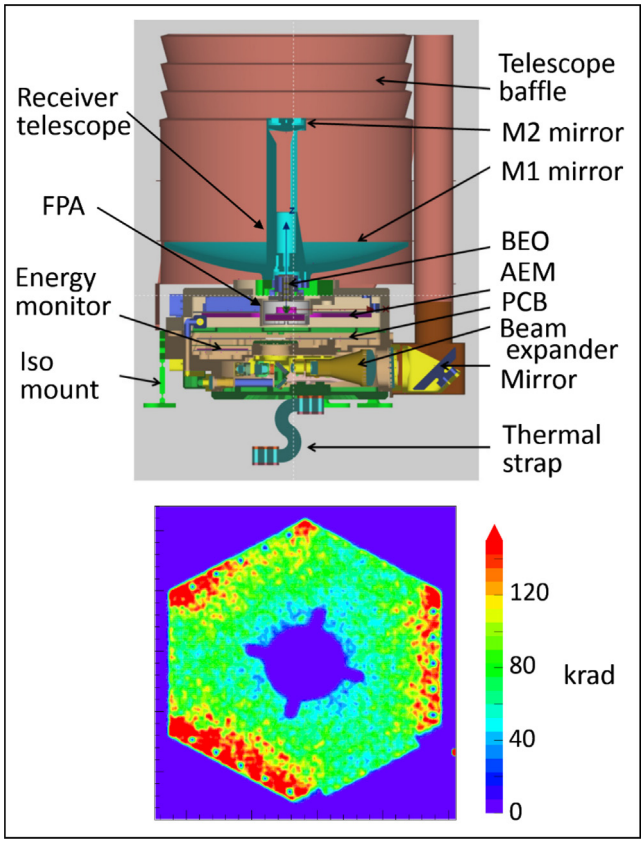

Fig. 15. Top: Geometric model used for radiation analysis. Bottom: Radiation intensity distribution in the AEM obtained through analysis.

ful ranging during Europa flyby; Case B: Successful ranging in Ganymede-centric orbit; Case C: Successful ranging data acquisition to show the presence or absence of Ganymede's internal ocean; Case D: Successful acquisition of ranging data with higher accuracy than Case C to confirm the presence or absence of Ganymede's internal ocean. In addition, the probability that the actual altimetry value falls outside the required value of ranging accuracy must be smaller than the probability of false detection. The SNR threshold of the return pulse waveform required to meet this requirement is defined as S_R (Required SNR).

First, S_R was obtained by simulating the received waveforms of GALA for the four cases A to D shown in Table 4. Specifically, multiple sets of simulated waveform data of the GALA return pulse were created. Based on the statistical variation of the peak timing, the probability of a false detection exceeding the specified range accuracy was determined. The waveform data of the simulated return pulses were created by a matched filtering process of {[standard waveform] + [normally distributed random noise]}. Next, the normally distributed random noise level was adjusted until the obtained probability of false detection equaled the required value shown in Table 4. The SNR of the confirmed received simulated waveform data was then set as S_R (Table 4), where SNR = [standard waveform peak value]^2 / [normally distributed random noise variance value] (Araki et al., 2019). The required value of range accuracy for Case A was set to 10 m.

Moreover, in order to verify the possibility of implementing S_R, the SNR calculated by considering the instrument performance and observation conditions of GALA, S_C (calculated SNR) needs to satisfy $S\_C > S\_R$ (Araki et al., 2019, Gunderson and Thomas, 2010). The performance degradation of APD in the radiation environment around Jupiter is important. Therefore, GALA-J experimentally evaluated the radiation-induced degradation of the APD by irradiating the APD with 2-MeV electron and 50-MeV proton beams, simulating the circum-Jupiter environment. The responsivity, gain (M), quantum efficiency (ε_{QE}), excess noise index (x), surface dark current (I_{DS}), and bulk dark current (I_{DB}) were re-evaluated by radiation tests (Araki et al., 2019; Kobayashi et al., 2016). By incorporating these results into the GALA performance model, $S\_C > S\_R$ was confirmed in all four cases A to D (Table 4) (Araki et al., 2019; Kobayashi et al., 2016).

Table 4
Requirements and calculated values for range accuracy.

Case	Mission phase	Altitude (km)	Range accuracy requirement (m)	Probability of false detection requirement	$S_{\_R}$	$S_{\_C}$
A*	Europa flyby observation	1300	–	< 0.2	> 22	23.2
B	Ganymede polar circular orbit observation (I)	500 ± 50	< 10	< 0.2	> 22	28.8
C	Ganymede polar circular orbit observation (II)	500 ± 50	< 2	< 0.1	> 43	202
D	Ganymede polar circular orbit observation (III)	500 ± 50	< 1	< 0.1	> 122	357

* In Case A, there is no range accuracy requirement from the project.

Currently, the flight hardware is being tested under realistic environmental conditions in various mission phases. These test results will be used to update the performance models to make them more accurate and realistic for use after launch.

3.2.8. Assembly, Tests, and delivery

The design, fabrication, and testing of the PFMs of BEO, FPA, and AEM (Figs. 10 and 14) were completed based on results of the development of the various models summarized in Table 3. First, functional tests, performance tests, and environmental endurance tests were executed for each PFM of BEO, FPA, and AEM. Then, the alignment of the BEO and FPA was adjusted using an instrument developed for this purpose. After that, the BEO, FPA, and AEM were assembled into a structure, and the qualification test for the entire assembly was conducted. Fig. 16 shows the thermal and vacuum tests and the vibration test. Table 5 shows the specifications of the environmental tests (thermal vacuum and vibration tests) for the PFM of BEO + FPA + AEM (acceptance level). The thermal balance test, DC magnetic field test, and partial discharge test were

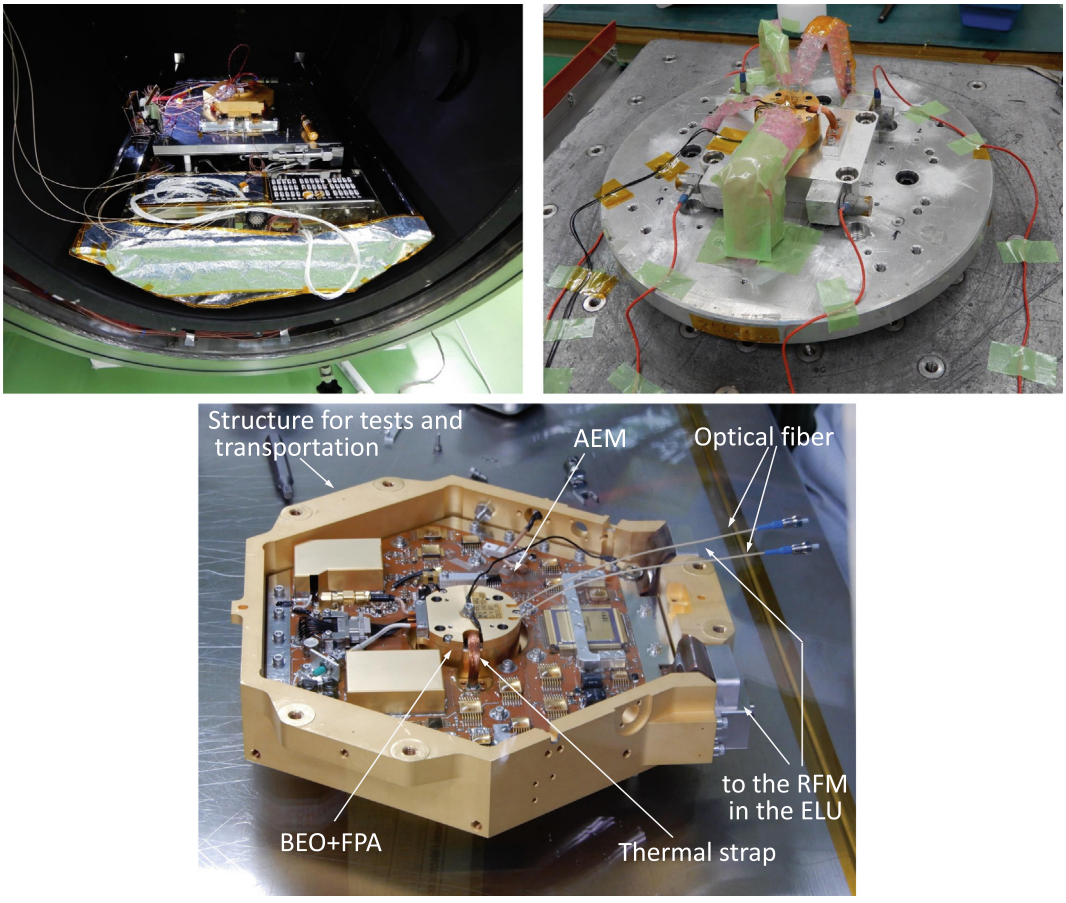

Fig. 16. Top left: Thermal test for assembled BEO + FPA + AEM (EM1-3). Top right: vibration test for BEO + FPA (EM1-3). Bottom: PFMs for BEO + FPA + AEM built into a structure for transportation and delivery to Germany.

Table 5
Specifications for environmental testing of PFM for BEO + FPA + AEM (acceptance level).

	Sine vibration test level	
	Frequency [Hz]	Acceptance level
Z-Axis	5–20	9.9 mm
	20–100	16 g
XY-Axis	5–20	6.6 mm
	20–100	10.7 g
		4 Oct/min
	Random vibration level (PFM: XY-axis)	
Frequenxy [Hz]	PSD [g^2/Hz]	Slope [dB/OCT]
20	0.007	–
140	0.075	3.607
160	0.952	57.042
200	0.952	0.000
220	0.451	−23.519
300	0.451	0.000
360	0.010	−62.637
600	0.010	0.000
2000	0.0001	−7.465
	Random vibration level (PFM:Z-axis)	
Frequency [Hz]	PSD [g^2/Hz]	Slope [dB/OCT]
20	0.0005	–
120	0.426	11.294
190	0.426	0.000
390	0.015	−13.950
440	0.326	76.494
600	0.326	0.000
650	0.050	−70.155
2000	0.0002	−15.094
	Thermal Vacuum test	
BEO + FPA	Non-operational High	85 °C
	Non-operational Low	−35 °C
	Operational High	50 °C
	Operational Low	−25 °C
AEM	Non-operational High	+65 °C
	Non-operational Low	−35 °C
	Operational High	+45 °C
	Operational Low	−5°C
Temperature		High: 0 °C to 3 °C
Tolerance		Low: 0 °C to − 3 °C
Thermal gradient		2 °C/min
Thermal stability		1 °C/hour
Number of cycles		1 cycle
Vacuum level		0.0013 Pa or less

completed in the environmental tests for the EM1-3, and therefore, not conducted for the PFM. After the tests were successfully completed, the BEO, FPA, and AEM were built into a structure for transportation and delivered to DLR in July 2020 (Fig. 16).

4. Mission status and remarks

The BEO, FPA, and AEM developed in Japan, the RFM developed in Switzerland, and the PCM developed in Spain were integrated in Germany. As of October 2021, the entire GALA is being tested. The EM1-3 of BEO + FPA and AEM sent from Japan is also being used for testing and adjustment. In the future, GALA-J plans to fabricate Flight Spare (FS) models of BEO, FPA, and AEM for the GALA project (Table 3). GALA is scheduled to be handed over to ESA in June 2021. The system will be installed in JUICE, and further tests will be conducted to launch it in 2023.

The GALA-J team learned fruitful lessons from the development of advanced laser altimeters through international work-sharing. It was essential to clearly define the interface, constraints, and all the requirements. On the other hand, adjustments had to be made if some tasks did not proceed according to the set plan. We have cleared the issue that reviews, phase-ups, and budget acquisition are not synchronized in Japan and Europe. In our international project, we met other issues, such as making in-house instrumentation and international product-and-quality assurance consistent, responding to numerous reviews and documentation in different laws and styles domestically and internationally, distance between Japan and Germany, and Covid-19. These lessons learned will be applied to the development of the next generation of advanced laser altimeters.

5. Summary

Almost 20 years after the Galileo spacecraft suggested the possibility of a subsurface ocean inside Jupiter's icy moons, the ESA-led development of JUICE has been underway. JUICE will be launched on an Ariane 5 rocket from the Guiana Space Center in 2023. It will reach the Jovian system in 2031 to perform flyby observations of Europa and Callisto and detailed observations of Ganymede from its polar orbit.

The Ganymede Laser Altimeter (GALA) is one of the scientific instruments onboard JUICE and the first laser altimeter to observe icy bodies. The core scientific objectives of GALA are as follows. (1) understanding ice tectonics based on topographic data, (2) understanding subsurface structures by measuring tidal response (including identifying the existence and characteristics of a subsurface ocean), and (3) understanding small-scale surface roughness and albedo. In addition, from the perspective of astrobiology, the scientific study of the subsurface ocean is of great significance.

To achieve these scientific objectives, GALA will repeatedly measure the distance (altitude) from orbit to the icy moon surface with high density and high precision. These measurements will capture topographic data, large-scale surface displacements and rotational changes across Ganymede's surface, and small-scale roughness and albedo. In these measurements, a laser pulse (start pulse, energy: 17 mJ, wavelength: 1064 nm, pulse width: 2.9 ns, nominal frequency: 30 Hz) will be irradiated on the icy moon surface from a nominal altitude of 500 km (nominal spot size: 50 m, spot interval: 50 m), and the reflected pulse (return

pulse) will be obtained. The distance will then be determined from the time lag between the start and return pulses. Finally, small-scale roughness and albedo will be analyzed from the intensity ratio of the return pulse to the start pulse and the pulse width broadening. The accuracy of the altitude measurement is approximately 1 m at points with good conditions.

The development of GALA has proceeded under the international cooperation of Germany (lead), Japan, Switzerland, and Spain. Within this framework, the Japanese team is responsible for developing the three modules of the receivers (BEO, FPA, and AEM). The BEO improves the optical SNR by applying spatial and bandpass filters to the return pulses collected by the receiving telescope. The FPA is equipped with an APD sensor module, which receives the light emitted from the BEO and converts its output into an analog electrical signal. The FPA is also equipped with optical fibers. A small fraction of the start pulse is input via optical fibers, and the output is converted into an analog electrical signal as well as the return pulses. The main function of the AEM is to receive the analog signal output from the APD sensor module and convert them into a digital signal. The AEM also controls the APD sensor module. In addition to the German team, GALA-J has developed software to simulate the performance of the entire GALA system (performance model). In July 2020, the PFMs of the BEO, FPA, and AEM were delivered from Japan to Germany.

Declaration of Competing Interest

The authors declare that they have no known competing financial interests or personal relationships that could have appeared to influence the work reported in this paper.

Acknowledgments

Development of GALA is proceeding through international collaboration between Germany, Japan, Switzerland, and Spain. The activities of GALA-J are supported by the Japan Aerospace Exploration Agency/the Institute of Space and Astronautical Science (JAXA/ISAS) and many other institutions. We are deeply grateful to all of the people involved with GALA-J and entire GALA.

The products of the GALA-J is being developed with many companies. We deeply thank everyone from NAITO DENSEI MACHIDA MFG. CO., LTD., Natsume Optical Corporation, MORIKAWA Co., LTD., YOKOHAMA-PRECISION CO. LTD., Fujitoku Co., Ltd., TOPCON CORPORATION, and OPTOQUEST CO., LTD.

References

Agostinelli, S. et al., 2003. Geant4- a simulation toolkit. Nuclear Instruments and Methods in Physics Research Section A: Accelerators, Spectrometers, Detectors and Associated Equipment 506 (3), 250–303.

Allison, J. et al., 2016. Recent developments in Geant4. Nuclear Instruments and Methods in Physics Research Section A: Accelerators, Spectrometers, Detectors and Associated Equipment 835, 186–225.

Allison, J. et al., 2006. Geant4 developments and applications. IEEE Transactions on Nuclear Science 53 (1), 270–278. https://doi.org/10.1109/TNS.2006.869826.

Araki, H., Tazawa, S., Noda, H., et al., 2009. Lunar global shape and polar topography derived from Kaguya-LALT laser altimetry. Science 323 (5916), 897–900. https://doi.org/10.1126/science.1164146.

Araki, H., Ishibashi, K., Namiki, N., et al., 2019. Performance model simulation of Ganymede Laser Altimeter (GALA) for the JUICE mission. Trans. JSASS Aerospace Tech. Japan 17 (2), 150–154. https://doi.org/10.2322/tastj.17.150.

Bland, M.T., Showman, A.P., 2007. The formation of Ganymede's grooved terrain: Numerical modeling of extensional necking instabilities. Icarus 189 (2), 439–456. https://doi.org/10.1016/j.icarus.2007.01.012.

Bolton, S.J., Lunine, J., Stevenson, D. et al., 2017. The Juno Mission. Space Sci. Rev., 213, 5–37. 10.1007/s11214-017-0429-6.

Calvin, W.M., Clark, R.N., Brown, R.H., Spencer, J.R., 1995. Spectra of the icy Galilean satellites from 0.2 to 5 um: A compilation, new observations, and a recent summary, j. Geophys. Res. 100, 19041–19048.

Cappuccio, P., Hickey, A., Durante, D. et al. 2020 Ganymede's gravity, tides and rotational state from JUICE's 3GM experiment simulation. Planet. Space Sci., 187. https://doi.org/10.1016/j.pss.2020.104902

Cavanaugh, J.F., Smith, J.C., Sun, X., et al., 2007. The Mercury Laser Altimeter Instrument for the MESSENGER Mission. Space Sci. Rev. 131, 451–479. https://doi.org/10.1007/s11214-007-9273-4.

Cheng, A. F., Barnouin-Jha, O., Zuber, M. T. et al. 2001. Laser Altimetry of Small-Scale Features on 433 Eros from NEAR-Shoemaker. Science, 292 (5516), 488–491. https://science.sciencemag.org/content/292/5516/488.

Daly, M.G., Barnouin, O.S., Dickinson, C., et al., 2017. The OSIRIS-REx Laser Altimeter (OLA) Investigation and Instrument. Space Science Reviews 212, 899–924.

de Kleer, K., Butler, B., de Pater, I., Gurwell, M.A., Moullet, A., Trumbo, S., Spencer, J., 2021. Ganymede's Surface Properties from Millimeter and Infrared Thermal Emission. Planet. Sci. J. 2, 5.

Enya, K., Kobayashi, M., Ishibashi, K., et al., 2018. Optical/mechanical design of the focal plane receiver of the Ganymede Laser Altimeter (GALA) for the Jupiter Icy Moons Explorer (JUICE) mission. In: Proc. SPIE 10698, Space Telescopes and Instrumentation 2018: Optical, Infrared, and Millimeter Wave. https://doi.org/10.1117/12.2312564.

Ester Program, NIST Standard Reference Database 124, National Institute of Standards and Technology (NIST), Physical Measurement Laboratory, 2017. http://physics.nist.gov/PhysRefData/Star/Text/ESTAR.html

Grasset, O., Dougherty, M.K., Coustenis, A., et al., 2013. JUpiter ICy moons Explorer (JUICE): An ESA mission to orbit Ganymede and to characterise the Jupiter system. Planet. Space Sci. 78, 1–21. https://doi.org/10.1016/j.pss.2012.12.002.

Gunderson, K., Thomas, N., 2010. BELA receiver performance modeling over the BepiColombo mission lifetime. Planet. Space Sci. 58 (1–2), 309–318. https://doi.org/10.1016/j.pss.2009.08.006.

Hirata, N., Suetsugu, R., Ohtsuki, K., 2020. A global system of furrows on Ganymede indicative of their creation in a single impact event. Icarus 352. https://doi.org/10.1016/j.icarus.2020.113941 113941.

Huang, Q., Ping, J.S., Yan, J.G., 2010. Chang'E-1 Laser Altimetry Data Processing. ADGEO 19, 137–149. https://doi.org/10.1142/9789812838162_0011.

Hussmann, H., Lingenauber, K., Kallenbach, R., et al., 2019. The Ganymede laser altimeter (GALA): key objectives, instrument design, and performance. CEAS Space J. 11, 381–390. https://doi.org/10.1007/s12567-019-00282-8.

Johnson, T.V., Yeates, C.M., Young, R., 1992. Space science reviews volume on Galileo Mission overview. Space Sci. Rev. 60, 3–21. https://doi.org/10.1007/BF00216848.

JUICE Team, "JUICE environment specification," ESTEC/ESA Noordwijk, The Netherlands, Technical Report, issue5, revision 6, JS-14-09, 2017.

Kamalakar, J. A., Laxmi Prasad, A. S. et al., 2009. Lunar Laser Ranging Instrument (LLRI): a tool for the study of topography and gravitational field of the Moon. Curr. Sci. 96, (4), 512-516. https://www.researchgate.net/publication/228371671.

Kamata, S., Kimura, J., Matsumoto, K., Nimmo, F., Kuramoto, K., Namiki, N., 2016. Tidal deformation of Ganymede: Sensitivity of Love numbers on the interior structure. J. Geophys. Res. Planets 121 (7), 1362–1375. https://doi.org/10.1002/2016JE005071.

Khurana, K.K., Pappalardo, R.T., Murphy, N., Denk, T., 2007. The origin of Ganymede's polar caps. Icarus 191, 193–202.

Kimura, J., Hussmann, H., Kamata, S., et al., 2019. Science objectives of the Ganymede Laser Altimeter (GALA) for the JUICE mission. Trans. JSASS Aerospace Tech. Japan 17 (2), 234–243. https://doi.org/10.2322/tastj.17.234.

Kivelson, M.G., Khurana, K.K., Volwerk, M., 2002. The permanent and inductive magnetic moments of Ganymede. Icarus 157 (2), 507–522. https://doi.org/10.1006/icar.2002.6834.

Kobayashi, S., Simone, D., Kobayashi, M., et al., 2016. JUICE/GALA-J (5): Radiation analysis for Ganymede Laser Altimeter (GALA) for the JUICE mission. In: Presentation at the Japan Geoscience Union Meeting 2016, Chiba, Japan. Abstract PPS11-P08.

Laforce, F., "Low noise optical receiver using Si APD", Proc. SPIE 7212, Optical Components and Materials VI, 721210 (6 February 2009); 10.1117/12.809071

Mizuno, T., Kase, T., Shiina, T., et al., 2017. Development of the Laser Altimeter (LIDAR) for Hayabusa2. Space Sci. Rev. 208, 33–47. https://doi.org/10.1007/s11214-015-0231-2.

Mizuno, T., Tsuno, K., Okumura, E., Nakayama, M., 2010. Evaluation of LIDAR System in Rendezvous and Touchdown Sequence of Hayabusa Mission. T. Jpn. Soc. Aeronaut. S. 53 (179), 47–53. https://doi.org/10.2322/tjsass.53.47.

Saur, J., Duling, S., Rothet, L., et al., 2015. The search for a subsurface ocean in Ganymede with Hubble Space Telescope observations of its auroral ovals. J. Geophys. Res. Space Physics 120 (3), 1715–1737. https://doi.org/10.1002/2014JA020778.

Schenk, P.M., 2002. Thickness constraints on the icy shells of the galilean satellites from a comparison of crater shapes. Nature 417, 419–421. https://doi.org/10.1038/417419a.

Schubert, G., Anderson, J.D., Spohn, T., McKinnon, W.B., 2004. Interior composition, structure and dynamics of the Galilean satellites. In Bagenal, F., Dowling, T.E., McKinnon, W.B. (Eds.), Jupiter: The Planet, Satellites and Magnetosphere. Cambridge University Press, Cambridge, Ch. 13, pp. 281–306, ISBN:. 978-0-521-81808-7.

Showman, A.P., Malhotra, R., 1997. Tidal evolution into the Laplace resonance and the resurfacing of Ganymede. Icarus 127 (1), 93–111. https://doi.org/10.1006/icar.1996.5669.

Smith, D.E., Zuber, M.T., Neumann, G.A., et al., 2017. Summary of the results from the lunar orbiter laser altimeter after seven years in lunar orbit. Icarus 283, 71–90. https://doi.org/10.1016/j.icarus.2016.06.006.

Smith, D.E., Zuber, M.T., Frey, H.V., et al., 2001. Mars Orbiter Laser Altimeter—Experiment summary after the first year of global mapping of Mars. J. Geophys. Res. Planets 106 (E10), 23689–23722. https://doi.org/10.1029/2000JE001364.

Smith, D.E., Zuber, M.T., Neumann, G.A., Lemoine, F.G., 1997. Topography of the Moon from the Clementine lidar. J. Geophys. Res. Planets 102 (E1), 1591–1611. https://doi.org/10.1029/96JE02940.

Steinbrügge, G., Stark, A., Hussmann, H., Sohl, F., Oberst, J., 2015. Planet. Space Sci. 117, 184–191. https://doi.org/10.1016/j.pss.2015.06.013.

Steinbrügge, G., Steinke, T., Thor, R., Stark, A., Hussmann, H., 2019. Measuring Ganymede's librations with laser altimetry. Geosciences 9 (7), 320. https://doi.org/10.3390/geosciences9070320.

Thomas, N., Hussmann, H., Spohn et al., 2021. The BepiColombo Laser Altimeter. Space Sci. Rev. 217:25. https://doi.org/10.1007/s11214-021-00794-y.

Zahnle, K., Schenk, P., Levison, H., Dones, L., 2003. Cratering rates in the outer Solar System. Icarus 163 (2), 263–289. https://doi.org/10.1016/S0019-1035(03)00048-4.

Ziegler, James F., SRIM Software, The stopping and range of ions in matter, 2013, http://www.srim.org/